The Thesis Committee for Joseph Yuchun Fu
Certifies that this is the approved version of the following thesis:

A study of low salinity water flooding in 1D and 2D

APPROVED BY
SUPERVISING COMMITTEE:

Supervisor:

Kishore K. Mohanty

Mojdeh Delshad

A study of low salinity water flooding in 1D and 2D

by

Joseph Yuchun Fu, B.S. Bio. Eng.; Ph.D.

Thesis

Presented to the Faculty of the Graduate School of

The University of Texas at Austin

in Partial Fulfillment

of the Requirements

for the Degree of

Master of Science in Engineering

The University of Texas at Austin

December 2011

Dedication

To my parents.

Acknowledgements

I would like to thank Dr. Kishore K. Mohanty for a chance to gain research experience in chemical enhanced oil recovery. I want to express my gratitude for his patience and guidance in tackling my research problems. I like to thank both Drs. Mohanty and Mojdeh Delshad for helping me with the editing of my thesis.

I would like to thank Dr. Eric Dao for guidance in experimental procedures and help with my research.

Finally I would like to thank all my lab-mates whose support and help make my time here at UT Austin a memorable experience.

Abstract

A study of low salinity water flooding in 1D and 2D

Joseph Yuchun Fu, M.S.E.

The University of Texas at Austin, 2011

Supervisor: Kishore K. Mohanty

The goal of this research was to study the effect of salinity on the waterflood of initially oil-wet clay-rich sand packs. Two one-foot long sand packs with 8% initial water saturation and 50% porosity were aged in crude oil for two weeks and flooded with either a low salinity (1000 ppm NaCl, pH 6.3) or a high salinity (20000 ppm CaCl, 20000 ppm MgCl, 20000 ppm NaCl, 20000 PPM KCl, pH 6.2) brine. 1D low salinity floods yield an incremental oil recovery of 15% and a significant change in the relative permeability. Initial breakthrough brine analysis showed that the low salinity flood results in more cation exchange activity compared to the high salinity case. A pH change of up to 1.4 point was witnessed for the high salinity case whereas the low salinity case had a 1.1 point pH change. The pH stayed below 7 in both low salinity and high salinity cases. The relative permeability of the low salinity case indicates a more water-wet state than that of the high salinity flood.

The 2D study focused on capturing the movement of the water saturation fronts in transparent 2D sand packs via digital recordings. Two-dimensional sand packs of the oil-aged clay-rich sands were constructed in plastic quarter 5-spot models. Secondary water floods were performed. Low salinity flooding yielded higher oil recovery at breakthrough than the high salinity case. There was more areal bypassing in the case of low salinity flooding. It was difficult to pack the 2D cells uniformly which affected the water floods.

Table of Contents

List of Tables

List of Figures

Chapter 1: Introduction and Motivation

Enhanced oil recovery is a technique to recover more of the oil that is left in the reservoir using chemical, thermal, or gas methods (Lake, 1989). It is garnering increasingly more attention as the price of oil increases because the demand for oil increases steadily and new oil supplies became harder and harder to find.

Low salinity water flooding is a relatively new technique where a low salinity water (salinity between 1000 and 4000 ppm with few divalent ions) is injected to recover additional oil over and above high salinity water injection (Lee 2010). In comparison to other methods of enhanced oil recovery, low salinity water flooding requires no additional up front cost if there is a source of injection water that is at a < 4000 ppm TDS concentration available within the vicinity. If there is no source of low salinity water, desalination of high salinity water can be implemented at a cost. In the past, some reservoirs were subjected to low salinity water flooding because of easy availability of that water without considering the effect of low salinity (Robertson 2007). It was not until decades later, that improvement from this process was recognized and published. By lowering the salinity of the injection water, it was found that up to 40% additional oil can be recovered (Lager 2008). The mechanism by which low salinity works is still not fully understood. It has been shown that the presence of kaolinite in the reservoir, the presence of divalent cations in the formation brine, and the presence of polar groups in the crude oil lead to improved recovery by low salinity flooding (Austad 2010).

The goal of this work is to improve the understanding of the low salinity flooding in clay-rich sand packs. A clay-rich sand and a crude oil have been identified which form an oil-

wet sand with a high salinity brine and a more water-wet condition with a low salinity brine. 1D sand packs were assembled and the effect of salinity on waterflood was determined. Then 2D transparent sand packs were constructed and the effect of salinity on saturation fronts were imaged. The background literature is reviewed in chapter 2. The methodology is described in chapter 3. The results are discussed in chapter 4. The last chapter lists the conclusions of this study.

Chapter 2: Background and Literature Review

Water flooding is a well-established practice in petroleum industry in which either produced brine or other readily-available water are injected into the reservoir to maintain reservoir pressure in order to stem off production decline. Besides the usual precaution taken of not injecting brine that can potentially damage the reservoir, such as the case of fresh brine that will cause clay swelling or sulfate-containing brine in barium-rich reservoir, little thoughts are given to the water chemistry that may occur when the injection brine composition is different from the reservoir brine composition. Recently, Tang et al. (1997) reported on the potential benefits of purposefully tailoring the injection brine salinity to affect a potential production increase. Since then, numerous other studies have been conducted to follow up on the investigation of the enhanced oil recovery potential of salinity manipulation. Yildez and Morrow (1999) conducted a core flood study with Berea sandstone and Prudhoe Bay crude oil showing a 16% oil recovery increase for a low salinity brine. Tang and Morrow (2002) noted that the low salinity behavior is accompanied by an increase in eluant pH, reduction in interfacial tension, reduction in relative permeability, shifting of the relative permeability curves corresponding to an increase in water-wetness, and production of fines. Additional low-salinity core flood studies have been carried out by different groups in secondary and tertiary mode and results were reported of increase oil recovery with decreased injection brine salinity (Webb et al. 2005; Agbalaka et al. 2008).

A study by Ligthelm et al. (2009) entailing core floods and Amott Imbibition studies found that reservoir wettability is closely linked to its salinity via the level of divalent

cation concentration; the higher the cations the higher the oil-wetness. They theorized that low salinity affects oil recovery through a change to a more water-wet state. Boussour et al. (2009) conducted studies of low salinity water flooding on reservoir and outcrop cores and found that low salinity recovery benefits are sensitive to temperature and that it would not work with some core/brine/crude oil/rock systems. Modeling of low salinity water flooding has been done by Jerauld et al. (2008). They have tied the low salinity effects to the relative permeability which are functions of wettability and saturation, and derived experimentally for both low salinity and high salinity conditions. Alotaibi et al. (2010) has studied low salinity behavior via contact angle and zeta potential measurement. They have found that different crude oil/rock/brine system wets differently and that zeta potential, which is a measure of wetness, tends to decrease as salinity decrease (Alotaibi et al. 2010). Zhang and Morrow (2007) have showed low salinity improvement in the secondary and tertiary modes for two reservoir cores with two different crude oils.

There are currently many successful examples of low salinity flooding on the reservoir scale. Field test of log-inject-log has been done to show 25-50% reduction in residual oil saturation (Webb 2004). Single well chemical tracer tests (SWCTT) done in Alaska's North Slope have given results of low salinity improvement resulting in increase in water flood recovery of 8-19% (McGuire 2005). The single well chemical tracer test was followed up by a field scale pilot at the Endicott field in North Slope of Alaska, which was a tertiary low salinity project entailing injection of a 0.4 pv low salinity slug (Seccombe 2008). The same author followed up with another study in the same Endicott

field which yielded incremental oil recovery of 10% of the total pore volume after 1.3 pore volume injection (Seccombe 2010). A field reservoir test in an unnamed field in Alaska reported an injection of 0.3 pore volume of un-optimized low salinity slug yielded a 2% decrease in S_{or} (Lager 2008). Low salinity flooding in the Omar field in Syria yielded an incremental recovery of 10-15% in stock tank oil initially in place (STOIIP) (Vledder 2010). In some cases, contaminated low salinity water from mining operations can be diverted for use as sources for waterflood. Core flood studies in tertiary mode have shown additional 3-9.5% recoveries for Tensleep and Minnelusa sandstones with synthetic coalbed methane water of 1,316 ppm (Pu 2008). Single well chemical tracer tests done in the Snorre field off the coast of Norway has shown little or no effect in enhanced oil recovery due to low salinity water flooding (Skrettingland 2010). This was attributed to the initial water wet condition of the reservoir with the high salinity brine. Low salinity water flooding could also work in conjunction with other enhanced oil recovery techniques. A study has pointed out that low salinity water flooding works well in conjunction of polymer flood considering polymers are sensitive to salinity and especially to divalent cations. A 5-10 times reduction in polymer concentration is expected with low salinity polymer flooding with desalination costs paid off in 1-4 years from the savings from the lower polymer concentration (Ayirala 2010).

Mechanism of Low Salinity Water Flooding

There are three main mechanisms attributed for the low salinity water flooding enhanced oil recovery response. They are fines migration, multicomponent ion exchange, and increased pH responses. When Tang and Morrow (1996) first reported the recovery

enhancement with low salinity water flooding, they have reported witnessing production of kaolinite fines along with the increase in production. They attributed the fine migration due to the low salinity induced formation damage and proposed it as the cause of the additional oil recovery. In the report, they gave evidence of increase in pressure drop and decrease in permeability which is logical with the clay production. However, later reports by the same authors mentioned low salinity improvement without fine production (Zhang and Morrow 2007). There are other authors who have reported no low salinity improvement despite great quantity of clay production (Boussour 2009) and those that reported low salinity improvement without fine production (Lager 2006). From these studies, it is apparent that in certain cases of studies, kaolinite fines did get dislodged and was produced in the eluant. Along with these fines, there is the possibility of additional oil being carried along and produced in the eluant. However, this mechanism cannot explain those cases where low salinity improvement was seen without the fine migration or the case of fine migration with no enhancement in oil recovery during low salinity flooding.

The pH increase has been proposed by different groups as the alternative driving mechanism for low salinity recovery improvement. Austad et al. (2010) has proposed novel chemical mechanism (Figure 2.1) in which directly adsorbed acidic and basic organic materials is desorbed upon contact with low salinity water according to the following figure.

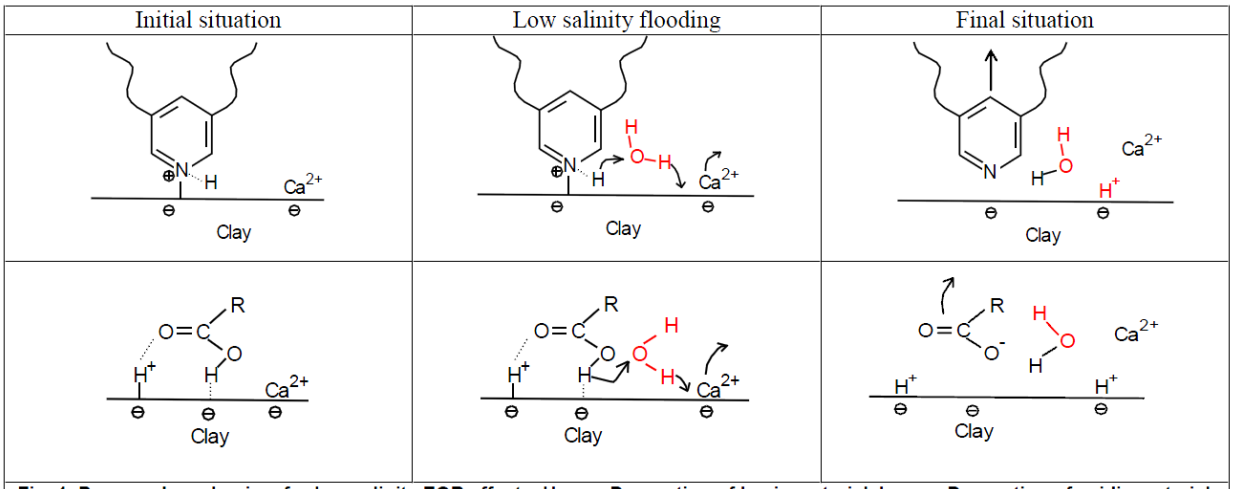

Fig. 1. Proposed mechanism for low salinity EOR effects. Upper: Desorption of basic material. Lower: Desorption of acidic material. The initial pH at reservoir conditions may be in the range of 5.

Figure 2.1: Chemical mechanism of acidic and basic material desorption (Austad 2010).

This group has proposed that injection of low salinity fluid disturbed the chemical potential equilibrium between the adsorbed divalent cations and the supernatant divalent cations (e.g. Ca^{2+}, Mg^{2+}). This difference in chemical potential acts as a driving force to reestablish the lost equilibrium by diffusion from calcium-rich rock surface to calcium-poor supernatant. The losses of calcium from the surface vacate a cation exchange site in which the protons from fresh invading water quickly take up, in the process release a hydroxide group according to the equation 1.

$$Clay\text{-}Ca^{2+} + H20 = Clay\text{-}H^{+} + Ca^{2+} + OH^{-} \quad (1)$$

This freed hydroxide caused a local pH increase which caused the following pH-sensitive acid/base reactions to occur as illustrated on the previous Figure 2.1 and in the following equation 2 and 3.

$$Clay\text{-}NHR_3+ + OH^{-} = Clay + R_3N + H_2O \quad (2)$$

$$Clay\text{-}RCOOH + OH^{-} = Clay + RCOO^{-} + H_2O \quad (3)$$

Austad et al. proposed this calcium-mediated desorption as the driving mechanism behind the low salinity behavior. They argued that the dominant acidic carboxylic groups and basic cyclic nitrogen compounds of the pyridine type found in common crude oil shown in Figure 2.1 have similar pKa of around 4.7-4.9 and thus will have similar adsorption and desorption behavior. They demonstrated their theory through an adsorption study. They showed that these acid/base adsorption/desorption follows the ordinary acid/base reaction which is strongly pH sensitive with adsorption of quinolone (basic material) and benzoic acid (acidic material) varying inversely with pH.

Austad et al. proposed that reservoir surface chemistry is much more complex with equilibrium adsorption of divalent cations, acidic and basic materials, and H^+ according to the affinity order.

$Li^+ < Na^+ < K^+ < Mg^{2+} < Ca^{2+} < H^+$

Basic and acidic organic materials have to compete with dissociated cations for active sites.

Austad's mechanism is subjected to the criticism that acid-base reactions with proton transfers are very fast due to low activation energy. But studies have found that low salinity behavior is sensitive to temperature (Boussard 2009).

Mcguire et al. (2005) proposed an alternative mechanism for low salinity behavior. They proposed that in-situ saponification happens when oil is exposed to higher pH low salinity brine according to the following equations 3 and 4.

$(RCOO)_3C_3H_5 + 3NaOH^- > 3(RCOONa) + C_3H_5(OH)_3$ (4)

Fat + alkali -> soap + glycerol

$2(RCOONa) + Ca(HCO_3)2^{-} > (RCOO)_2Ca + 2(NaHCO_3)$ (5)

Soap + hardness -> insoluble soap curd

This soap in equation 4 reduces the interfacial tension, and the elevated pH increases the wettability of the reservoir. The low salinity water being soft generally, does not have the high enough divalent cation concentration to precipitate out the soap generated in this manner. McGuire et al. offer as evidence the data reported by Tang and Morrow (2002) which show the eluant pH increased by 2 point from pH of 8 to 10 and the reduction of interfacial tension reported along with the increased oil recovery. Criticisms of this proposed mechanism are numerous. This present study reports a low salinity incremental oil recovery without approaching the pH 9, which is the threshold pH needed for the in-situ saponification similar to the alkaline flood described by McGuire to occur. Additionally, alkaline flood requires a high AN (>0.2) (Ehrlich and Wygal 1997). Fields in North Sea which this alkaline flooding mechanism is attributed to the low salinity flooding recovery improvement there have very low acid number in their crude (AN < 0.05). Others have point out that the high pH required for this alkaline-flood like low salinity flood mechanism to occur is quite impossible in the field due to the fact that most fields are acidic for their presence of H_2S and CO_2.

Lager et al. (2006) published a work proposing multi-component ion exchange as the dominant mechanism driving low salinity water flooding recovery improvements. From the list of mechanisms given by Sposito (1989) for organic matter adsorption onto clay material, the dominant four: cation exchange, ligand bonding, and cation and water

bridging, Lager (2006) narrow it down to Van Der Waals interactions, ligand exchange and cation bridging as the dominant adsorption mechanism (Figure 2.2).

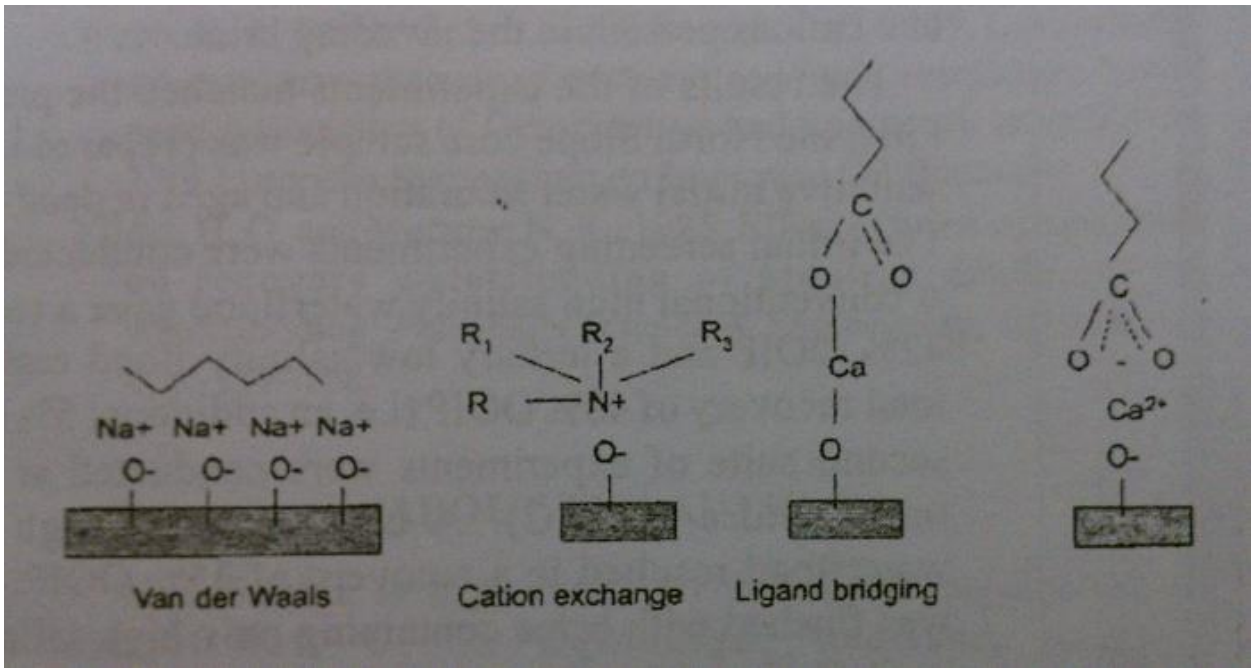

Figure 2.2: Representation of the dominant adhesion mechanism between clay and crude oil (Lager et al. 2006)

They observed that divalent cation concentrations are lowered in the affluent in low salinity flooding. From this observation, they linked the importance of divalent cations to the low salinity flooding improvements. Out of the four proposed mechanism illustrated, only cation bridging takes into account calcium. So by the process of elimination, they theorize that cation bridging is the dominant mechanism driving the low salinity improvement. Lager et al. propose that polar components in the crude form organo-metallic complexes with the calcium present in reservoir at the rock surface making the surface oil wet, when low salinity brine is being injected into the reservoir, the free cation

in the injection brine exchange with the bound organo-metallic complex and thus freeing the cation-bridge bound oil. To test their theory, they conducted a core flood in which a core is pre-flooded with high Na brine until only traces of Ca and Mg are left. Then they flooded the core with oil and aged the core. They proceeded with a High Na (no calcium or magnesium) flood and got a 42% recovery at 25 degree C and 48% at 102 degree C. Additional flood of low salinity of Na only (no calcium or magnesium) yielded 5% additional recovery at room temperature and no additional recovery at 102 degree C. Subsequent flooding of low salinity brine containing only Ca and Mg produces no additional recovery. This gives a strong indication that low salnity improvement is mainly derived from cation-bridging bound oil. In the absence of this particular mechanism of clay-oil adsoption, low salinity improvement is not seen for the high temperature case.

Lager et al. have followed with reports of studies of water layer thickness by small angle neutron scattering and X-rays. They reported that by using these two methods, they were able to observe that the electrical double layer is expanding as the salinity decrease for both sand and clay-like surfaces with the expansion being more drastic for divalent cations on clay like surfaces (Lee et al. 2010). They thus provided quantitative data for double layer expansion and incorporatedit as evidence for their MIE theory to explain the low salinity improvement (Figure 2.3).

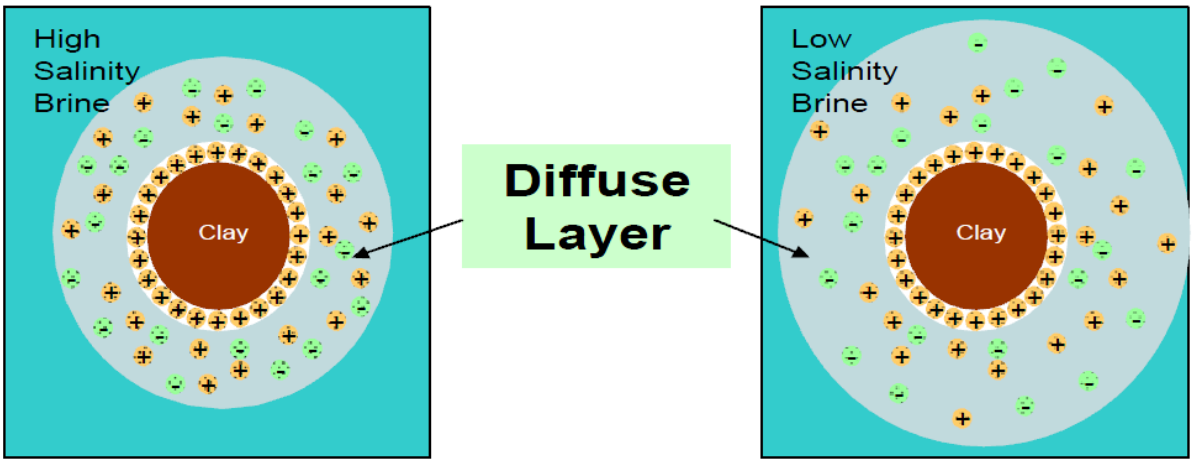

Figure 2.3: Expansion of electric double layer

Criticism of Lager's multicomponent ion exchange theory for low salinity water flooding improvements is the theory's inability to go beyond the cation-bridge bound organics. For positively-charged organics adsorbed on the rock matrix, they are lumped in with the cation-bridge bound type and are thought to be desorbed with them during low salinity flooding. References from soil science have reported that this cationic molecule would be much more adsorbed in distilled water than high salinity case (Wang 1990; Hedge and Hare 1987).

Tripathi et al. (2007) gave three models of relative permeability as a function of salt concentration for the purpose of using them to test for instability associated with wettability alteration during low salinity flooding. The models are expressed by Corey's function. Corey's parameters are assumed to be a function of salinity.

$$k_{rw} = k_{rwo}\,(S_w^*)^{nw}$$

$$k_{ro} = k_{roo}(1-S_w^*)^{no} \qquad (6)$$

$$S_w^* = (S_w-S_{wr})/(1-S_{wr}-S_{or})$$

The models are layered in complexity with one building onto another. The first modeled relative permeability through lowering the residual oil saturation (K_{rwo} = 0.5, k_{roo} = 1, S_{wr} = 0.2, n_w = 3, n_o = 2).

$$\begin{aligned} S_{or} &= 0.1, && C_s < C_{s1}\ (1000\ ppm) \\ &= 0.1+0.2(C_s - C_{s1})/(C_{s2}-C_{s1}), && C_{s1} < C_s < C_{s2} \\ &= 0.3, && C_s > C_{s2}\ (7000\ ppm) \end{aligned} \quad (7)$$

The second model added on alteration of end-point water permeability.

$$\begin{aligned} K_{rwo} &= 0.5, && C_s < C_{s1}\ (1000\ ppm) \\ &= 0.5-0.4(C_s - C_{s1})/(C_{s2}-C_{s1}), && C_{s1} < C_s < C_{s2} \\ &= 0.1, && C_s > C_{s2}\ (7000\ ppm) \end{aligned} \quad (8)$$

The third model added on changes to the relative permeability exponents. At high salinity, n_w = 3, n_o = 3, S_{or} = 0.3; at low salinity, n_w = 4, n_o = 2, S_{or} = 0.1 (These are constant: k_{rwo} = 1, k_{roo} =1, S_{wr} = 0.15)

The solution for1D displacement is solved analytically for model 1. Neglecting capillary pressure and gravity, 1D displacement of oil by brine is represented by

$$\phi \frac{\partial S_w}{\partial t_D} + u \frac{\partial f_w}{\partial x_D} = 0 \quad (9)$$

With fractional flow of brine expressed as

$$f_w = \frac{k_{rw}/\mu_w}{k_{rw}/\mu_w + k_{ro}/\mu_o} \quad (10)$$

The transport of salt neglecting dispersion, diffusion, and adsorption is

$$\phi \frac{\partial (S_w C_s)}{\partial t_D} + u \frac{\partial (f_w C_s)}{\partial x_D} = 0 \qquad (11)$$

With initial and boundary conditions

$S_w(X_D) = 1 - S_{or}$ @ $t_D = 0$, $0 \leq X_D \leq 1$ (12)

$fw(t_D) = 1$@$x_D = 0$, $t_D \geq 0$ (13)

Solving equations 9-11 for model 1, the result is shown through Figures 2.4-2.6.

Figure 2.4 shows the saturation profile at 0.5 PV injected with viscosity ratio assumed of 3.3.

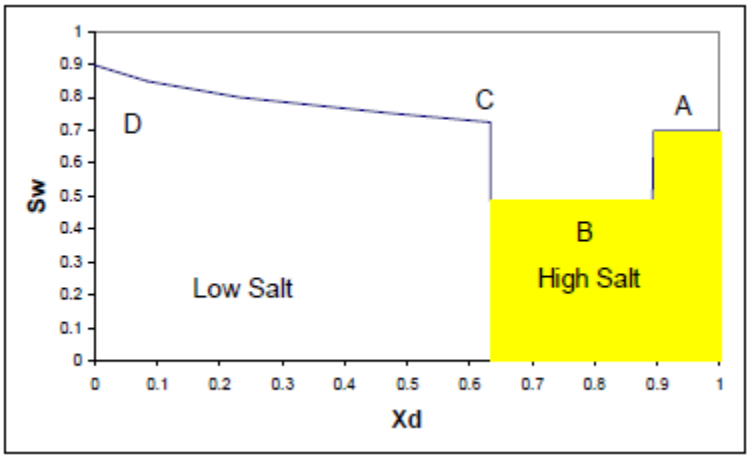

Figure 2.4. Saturation profile at 0.5 PV, Model 1 (Tripathi 2007).

The saturation profile showed two saturation shocks, AB and BC, and one concentration shock at BC. Saturations at these shocks are obtained by drawing the tangent line at point C across the two fraction flow curves (Figure 2.5). The low salinity phenomenon is seen as a shift to a more water-wet stat at breakthrough for secondary flow for low salinity flood.

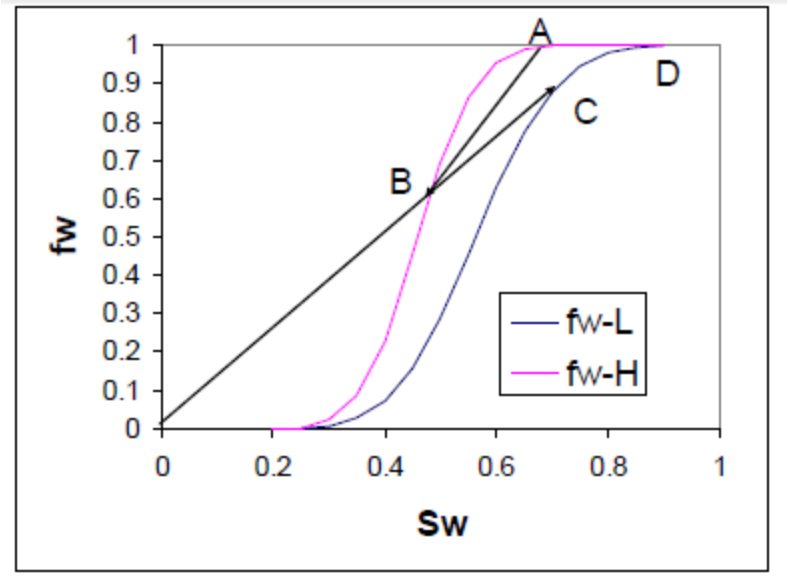

Figure 2.5: Fractional flow and shocks for Model 1(Tripathi 2007).

Figure 2.6 shows the total relative mobility ($k_{rw}/\mu_w + k_{ro}/\mu_o$) profile at 0.5 PV injected. Total mobility increases across the high salinity shock front and decreases across the low salinity shock front signifying stability across high salinity shock and instability across low salinity shock. Tripathi reported similar results for both secondary and tertiary low salinity flood.

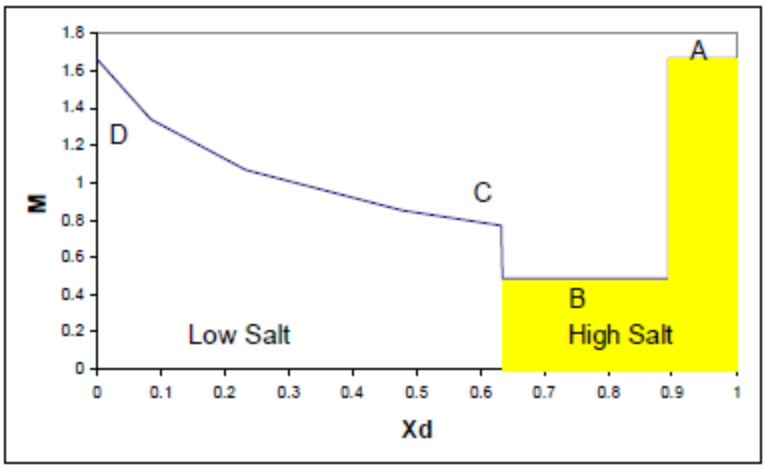

Figure 2.6: Total relative mobility profile at 0.5 PV, Model 1 (Tripathi 2007).

Due to the adverse total relative mobility, instability in 2D flow is expected. Figure 2.7 shows the effect of viscosity ratio on saturation profile of Model 1. As viscosity ratio increase, the width of the oil bank decrease as the speed of low salinity shock increases while that of high salinity shock decreases. For the cases shown in Tripathi's study, the threshold viscosity ratio is 10 under which the low salinity shock is unstable, and fingering may occur. According to Tripathi et al., Low salinity flood are expected to be mildly unstable according to their salinity dependent relative permeability models because of the low mobility ratio across the low salinity shock front and presence of capillary pressure.

In the following chapters, chapter 3 will discuss the materials and methods involved in this study. Chapter 4 will go into the results and discussions. Chapter 5 will be the conclusions.

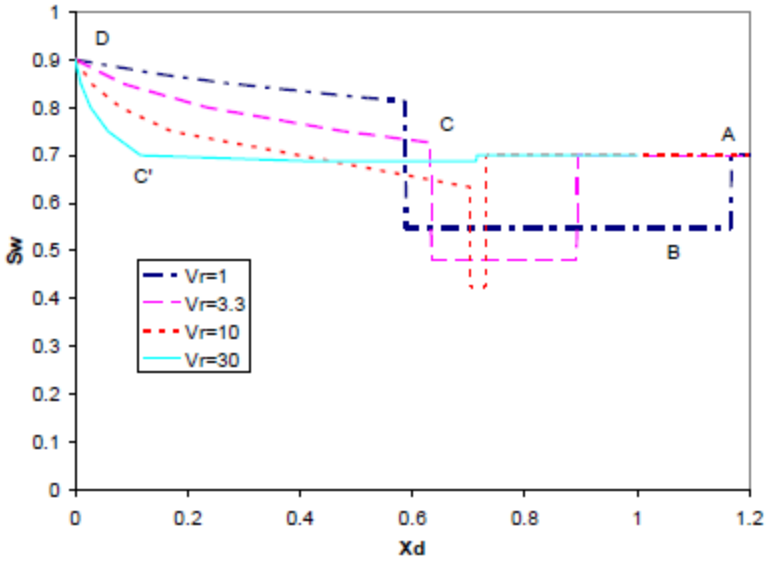

Figure 2.7: Effect of viscosity ratio on saturation profile at 0.5 PV injection, 1D flow, Model 1 (Tripathi 2007)

Chapter 3: Experimental Procedures and Materials

3.1 MATERIALS
3.1.1 Aqueous Phases
3.1.1.1 High Salinity Brine

Salts used in this study were all acquired from Fisher Scientific (NaCl, $CaCl_2$, $MgCl_2$, and KCl). There were several types of high salinity brines that were used in the beginning of this project, but at the end, only one brine composition was selected. This brine was chosen to yield an oil-wet sand pack after aging with a crude oil. This high salinity (HS) brine was used in most of the sand pack experiments. The composition of this HS brine is listed in Table 3.1.

Components	Concentration (ppm)	Cation (ppm)	Anion (ppm)
NaCl	20000	7868	12132
MgCl	20000	7226	12774
KCl	20000	5121	14879
CaCl2	20000	10490	9510

Table 3-1: The composition of high salinity (HS) brine

The HS brine listed in Table 3-1 has a density of 1.05 g/ml, a viscosity of 1 cp at room temperature and 0.5 cp at 80 degree C, and pH of about 6.4.

3.1.1.2 Low Salinity Brine

The composition of the low salinity (LS) brine was chosen to be 1000 ppm NaCl in deionized water. The viscosity of this brine is 0.98 cp at room temperature and 0.5 cp at 80 degree C; the pH is about 6.6. In the literature, low salinity behavior was reported for

TDS values up to 5000 ppm. Usually in the field, the low salinity brine is made by the dilution of field brines; so it includes traces of the divalent cations. For the purpose of this study, the divalent cations (e.g. calcium and magnesium) were intentionally left out. This was done with the presumption from literature review that the role of calcium and magnesium is vital for low salinity water flooding. Thus the divalent cations were left out to see the effect on oil recovery. However, contamination from the pump made elimination of divalent cations from the low salinity brine impossible. So in the low salinity brine used in this study, up to 50 ppm of other cations including potassium, calcium, and magnesium are present unintentionally.

3.1.2 Choice of packing

From the literature, low salinity behavior has been reported for predominantly kaolinite-bearing reservoirs. But studies have found that illite and montmorillonite have also been found to have low salinity improvements (Cissokho 2009).

Table 3.2 lists some of the properties of clay minerals. Kaolinite has a relatively low cation exchange capacity and low surface area compared to the other clays. Despite these characteristics, kaolinite was still chosen to be the mineral for further studies because it does not swell much upon hydration. We used a mineral called cristabollite which is a mixture of sand and about 30% clay. The amount of kaolinite in cristabollite is higher than that in sandstones used in other low salinity studies. This higher content can amplify the effect of low salinity flooding if the correlation between kaolinite and low salinity effect is true (Seccombe 2008).

Property	Kaolinite	Illite/Mica	Montmorillonite	Chlorite
Layers	1:1	2:1	2:1	2:1:1
Particle size (micron)	5-0.5	large sheets to 0.5	2-0.1	5-0.1
Cation exchange cap. (meq/100g)	3-15	10-40	80-150	10-40
Surface area BET-N_2 (m^2/g)	15-25	50-110	30-80	140

Table 3.2: Properties of actual clay minerals (International Drilling Fluids (IDF), 1982)

Kaolinite source was chosen to be a rock mineral mixture of kaolinite cristobalite from Wards Natural Science. This is a whitish flaky type of rock with soft texture (Figure 3.1). Kaolinite cristobalite is a rock that is roughly 30% clay (mainly kaolinite) with a chemical structure of $Al_2Si_2O_5(OH)_4$ and 70% cristobalite, which is just another polymorph of silica with chemical structure SiO_2. The rock came in buckets of 25 pounds lots, in cobble to boulder size fragments. Intensive processing was required to break the rock down to packing sized materials suitable for sand pack experiments.

Figure3.1: Kaolinite cristobalite

3.1.2.1 Kaolinite Cristobalite Processing

Kaolinite cristobalite fragment were initially hammered down to cobble sized pieces and fed into a manual bench top jaw crusher (Figure 3.2) that crush the rock farther down to pebble size pieces.

Figure 3.2: Jaw crusher

At this point, the rocks were fed into an Oster 14 speed blender with a glass jar and a 350W motor. The blender was turning on high first before the rock was fed from the top spout opening with a funnel while the blade is turning. The rock is turned into sand size or smaller particles afterwards. The processed sand is sieved through a stack of sieve from Hogentogler Inc. ranging from mesh size 30 to 400 with corresponding particle diameter 600 to 38 microns using RO-TAP model E Test Shaker (Figure 3.3) on fine for 10 minutes.

Figure 3.3: Ro-Tap Test Shaker

These processed sands are highly irregular due to their natural conchoidal fractures and artificial lack of normal weathering. An example of these sands' irregular shapes can be seen in Figures3.5-3.6, and it's especially clear under 11x zoom in Figure using Olympic Stage Microscope SZ-CTV (Figure 3.4).

Figure 3.4: Olympus Stage Microscope

Figure 3.5: 50 mesh (300 um) kaolinite cristobalite sand under 3x zoom

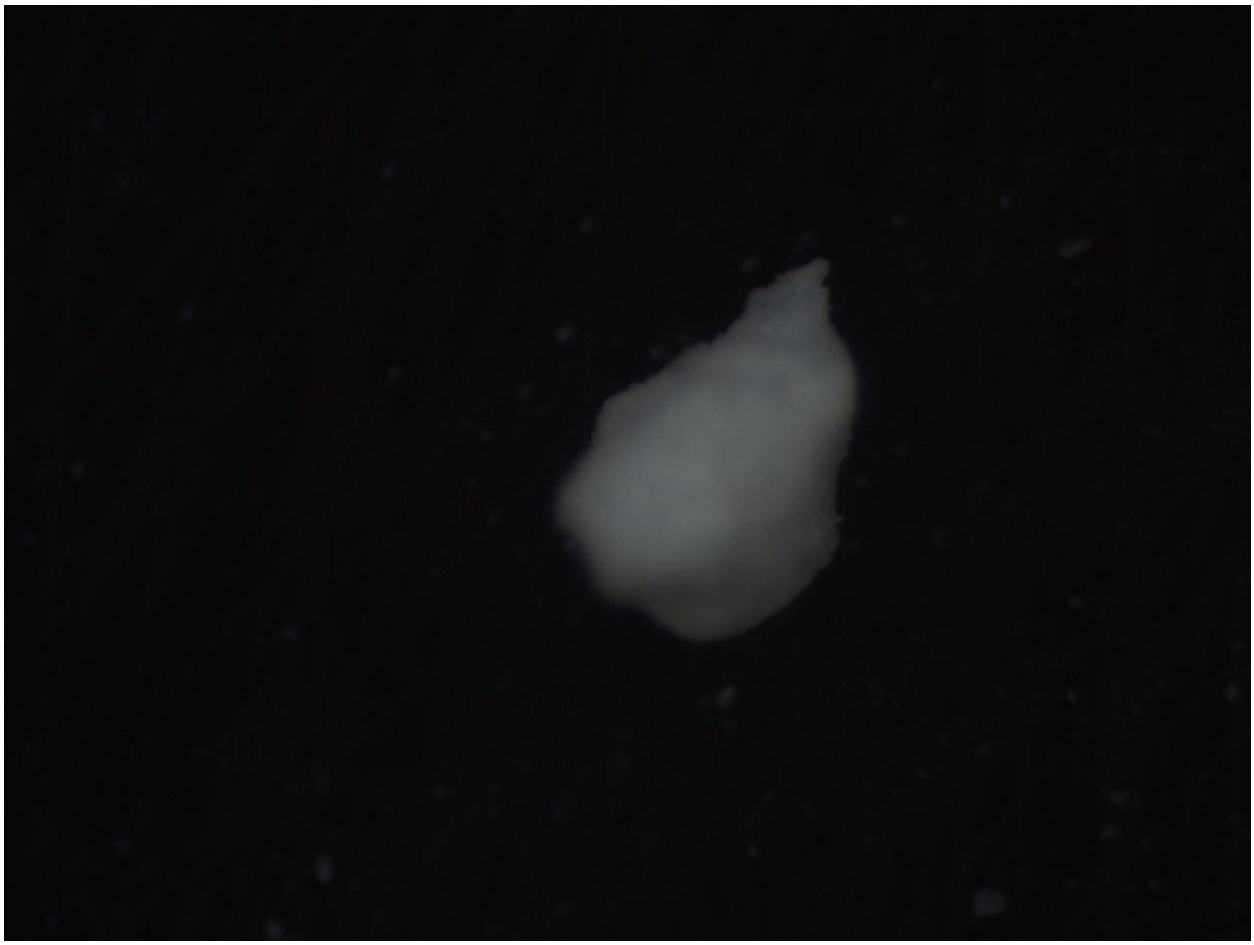

Figure 3.6: 50 mesh kaolinite cristobalite under 11x zoom

3.1.3 Choice of Oil

Only the oils in our laboratory were tested. There were a total of four different oil that were screened initially to find one that makes clay-rich sands oil-wet.

3.1.3.1 Oil Screening

Four different oils were screened initially in a qualitative manner to see which one would yield the following conditions needed for low salinity experiments. Kaolinite and cristobalite sands were exposed to the high salinity brine and spun using a centrifuge at 5000 rpm for three reps of thirty minutes to get rid of excess brine followed by incubation

in different oil for a week at 80 degree C. Afterwards the sand was taken out and put into High Salinity and Low Salinity Brine and incubated at 80 degree C. Pictures of the sands were taken at different aging periods and they are shown in Figure 3.7 and 3.8.

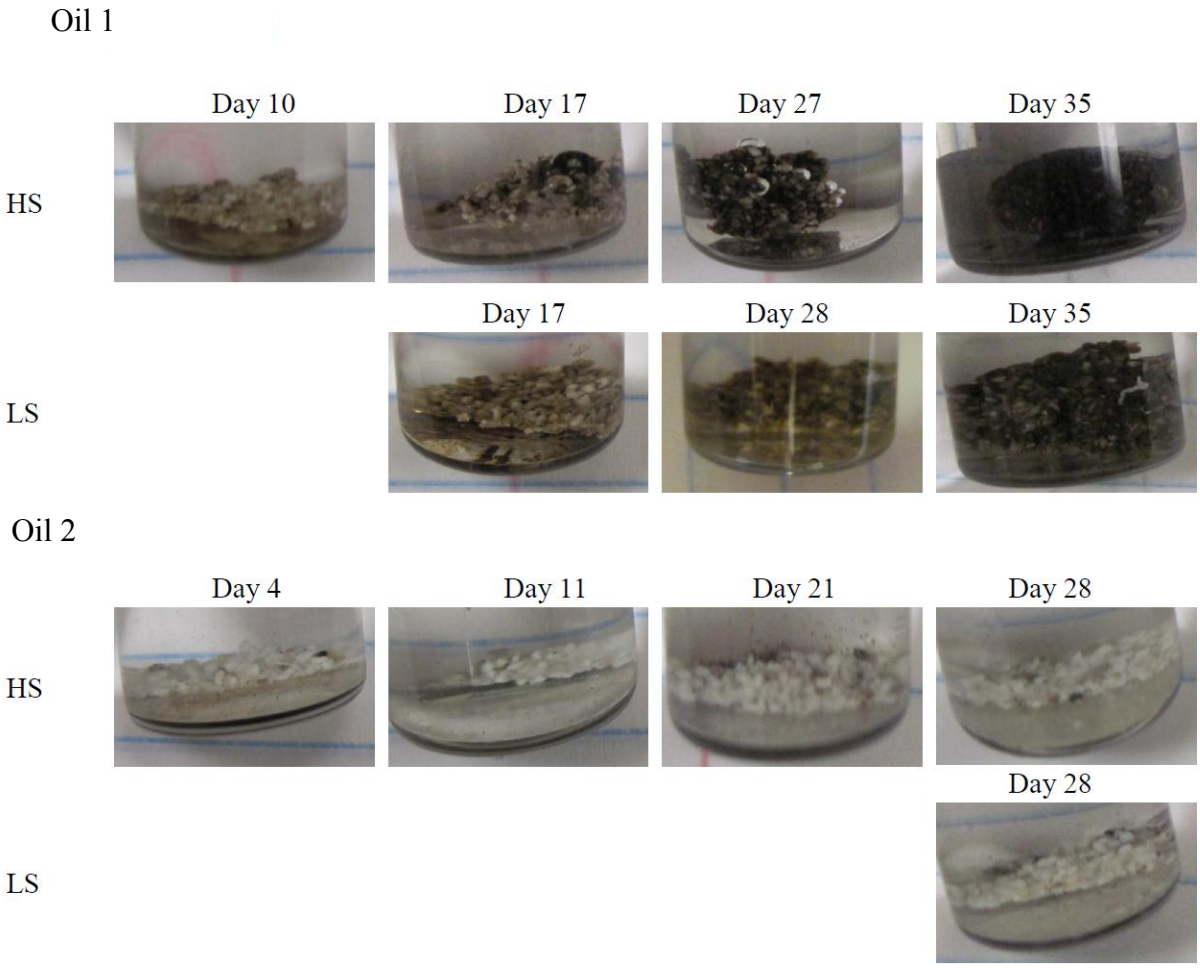

Figure 3.7: Oil 1 and oil 2: Oil-aged sand in HS and LS brines

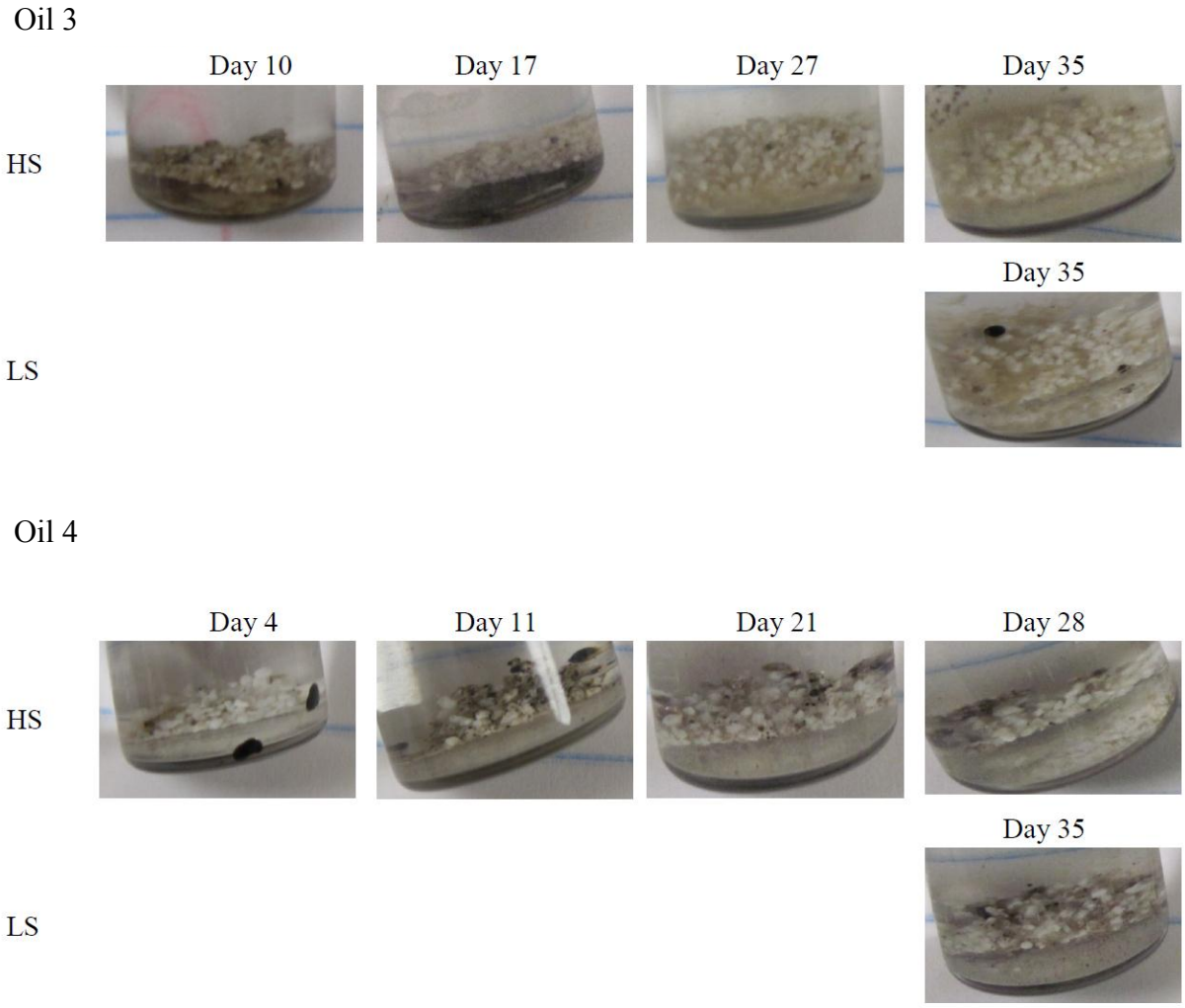

Figure 3.8: Oil 3 and oil 4: Oil-aged sand in HS and LS brines

Based on the qualitative results above, oil 1 was selected to be the oil for this wettability study.

3.1.4. Choice of packing size and size distribution

Sand packs were initially packed with uniformly sized kaolinite crystobalite sands. Due to the irregularity of the kaolinite crystobalite sand structure, the sand pack had a very loose packing yielding an extremely high porosity. The highly porous medium yielded a

very high permeability in the hundreds of Darcy range challenging the limits of the pressure transducer's ability to measure the pressure data in the linear range. Figures 3.9 shows the porosity and permeability value of the 1 D sand pack at different mesh size. Figure 3.10 shows the pressure drop for the different sand pack at various flow rates.

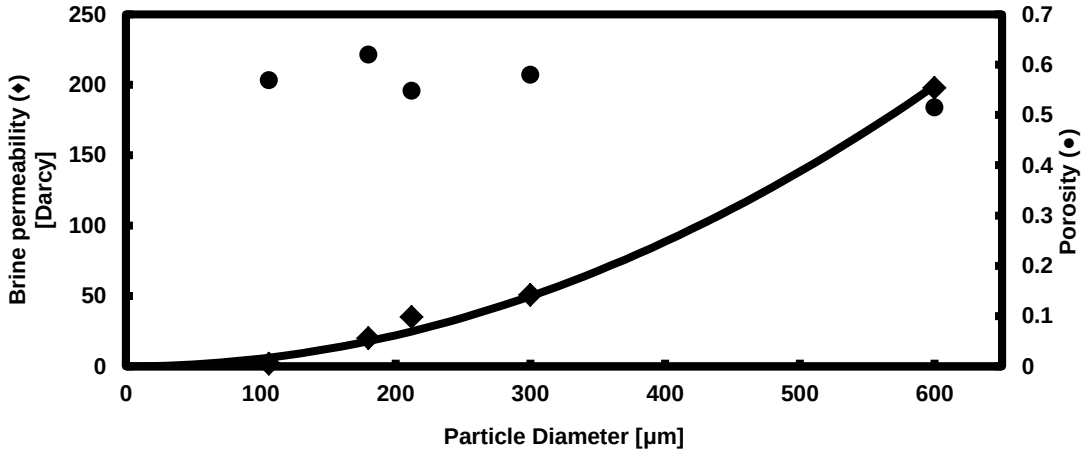

Figure 3.9: Brine permeability and sand pack porosity vs. particle size

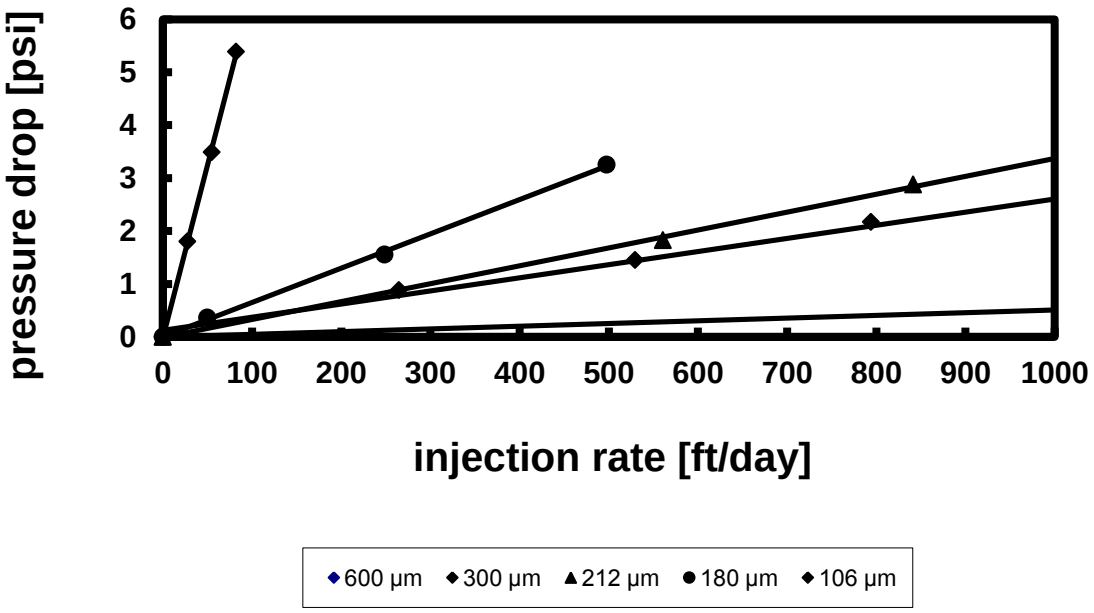

Figure 3.10: Pressure drop vs. flow rate for different sand diameters

In Figure 3.11 the tortuosity of the various sand packs was calculated using Carmen-Kozeny equation

$$\tau = \frac{D^2 \varphi^3}{72k(1-\varphi)^2}$$

and a fit is generated as a function of the particle size.

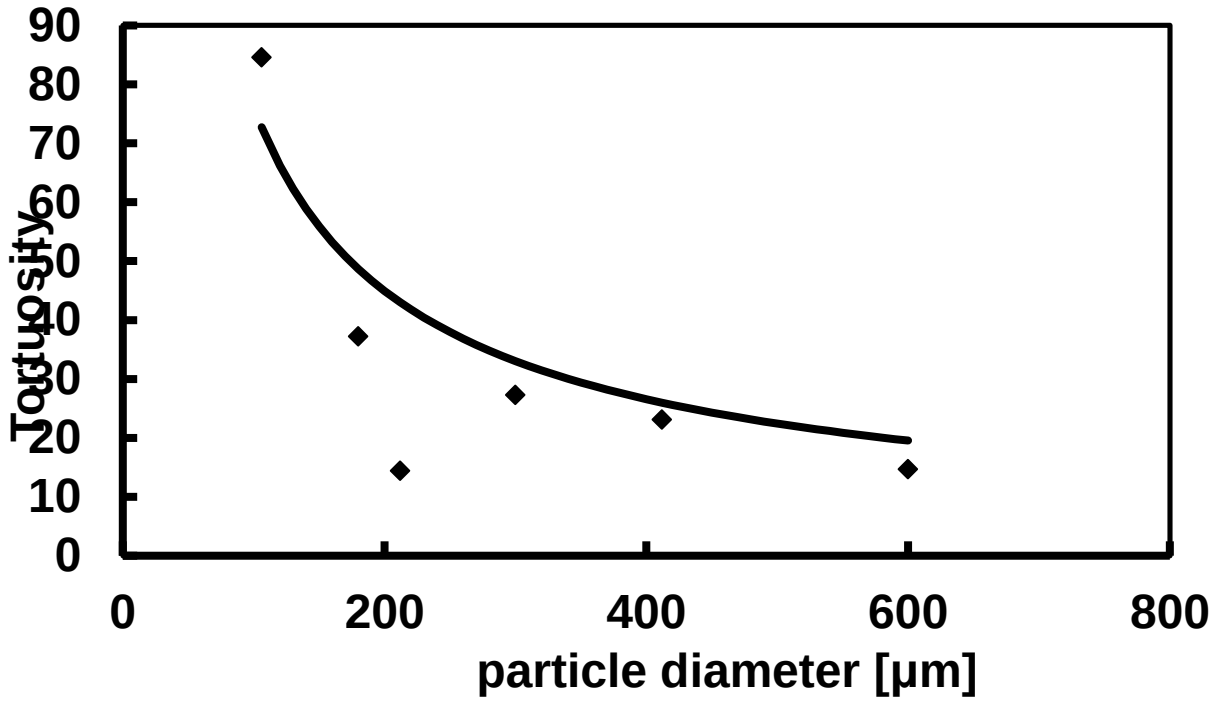

Figure 3.11: Tortuosity vs. particle diameter

In order to have a sand pack that is within the working linear range of the Rosemount pressure transducer used, the sand size is limited to the lower diameter range. The porosity of the sand pack is a weak function of the diameter of the kaolinite crystobalite sands; however the sand pack permeability is a strong function of the size. With the goal of achieving lowered permeability and thus a measurable pressure drop within the capability of the pressure transducer, the sand pack is packed with a distribution of sand size mimicking what is likely to occur in nature (Figure 3.13).

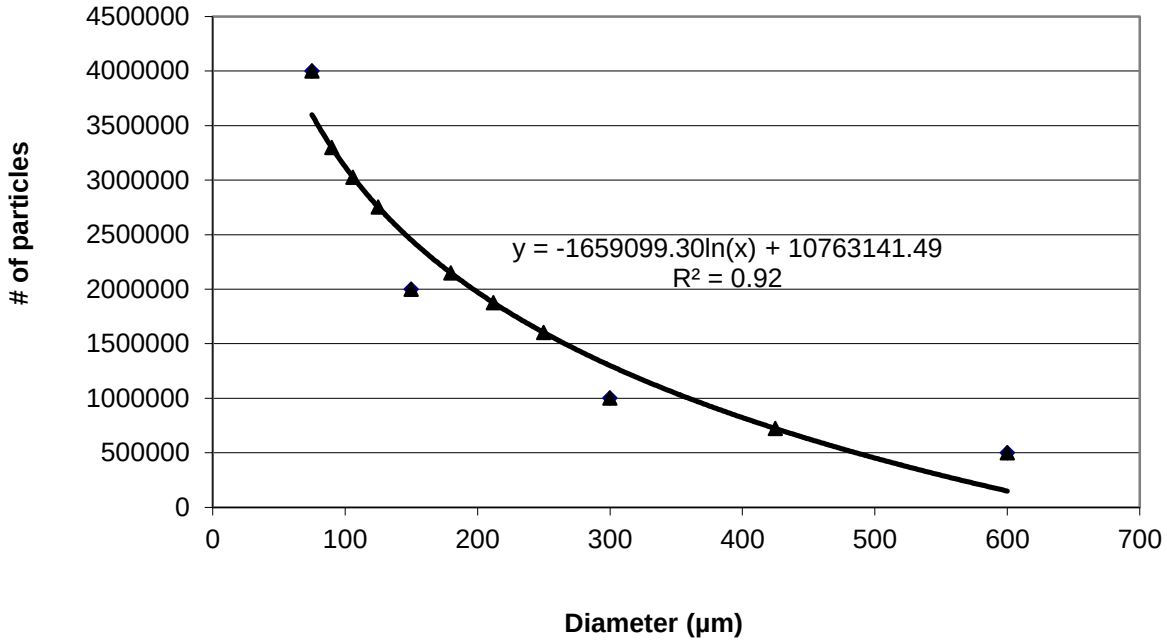

Figure 3.12: Number of particles vs. particle diameter for a log normal distribution

The sand pack is packed according to the following equation illustrated in Figure 3.12.

$$N = -1659099.3lnD + 10763141.5$$

N is the number of particles and D is the size of the particle in microns. The equation is based on the idea that one bigger sized particle splits uniformly to two smaller sized particles and so on according to Figure 3.13 in a log normally distributed way.

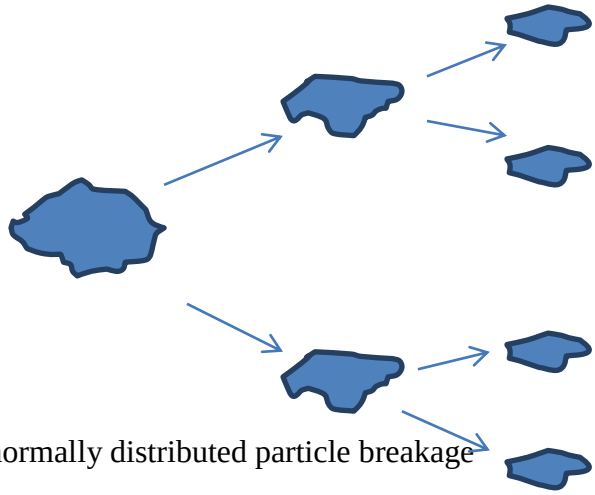

Figure 3.13: Log normally distributed particle breakage

In order to have workable reproducibility, these ratios of fragments at each mesh size are related to volume. This is done painstakingly by counting each mesh size up to a certain volume and scaling that volume up by a scale factor. To convert from number of particles to volume of uniformly sieved particles needed, the following empirical equation is found to be a good fit.

$$V = \pi N D^3$$

V is volume of sieved particle needed in ml, N is the number of particles needed from the previous equation, and D is the size of the particle in meters. The equation produced a ratio of volume as a function of size according to Table 3.3.

Mesh	Particle size (micron)	volume ratio needed (ml)
30	600	137
40	425	70.31949442
50	300	34.25
60	250	31.76230747
70	212	22.67487277
80	180	15.88728211
100	150	8.5625
120	125	6.819499954
140	106	4.57180883
170	90	3.049372766

Table 3.3: Volume ratio for different particle size

Sand pack with sands of varying diameter at the ratio listed in Table 3.3 was found to be yielding lowered porosity and acceptable permeability and pressure drop. After initial experiments showing tighter than expected permeability, sand packs of mesh size 50-100 was chosen as the range to work with that yield a permeability with associated pressure range in the acceptable linear region but not so tight as to cause immediate blockage during flooding.

3.1.5 Sand Pack

1D sand pack tube was bought from Autoclave Engineering Inc (Figure 3.14). The length of the sand pack was 1ft and the diameter was 0.55 inch. The fitting used for 1D sand pack were the high pressure valves from High Pressure Equipment Company that can tolerate up to 10000 psi of pressure.

Figure 3.14: 1D sand pack

2D sand pack

Initially the 2 D sand packs were designed to have roughly 1580 mL capcity at 12” x 12” x 0.5”. The initial design has three plates all made of polycarbonate (Figure 3.15).

Figure 3.15: Initial 2D sand pack design; top (and bottom) plate (left), and middle plate (right)

This design had several problems. The first problem was that the middle plate being thinner and made of polycarbonate was fragile and the inlet and outlet ports are prone to threading lost. Falls and exposure to heat weakens the polycarbonate so that fractures were common and resulting leaks compromised the seal. The most severe problem with the initial design was the necessity of more oil as it has a high capacity. Because of these problems, the initial design was abandoned when the oil used for the project was no longer sufficient to finish the experiment. Therefore, a low capacity 2D sand pack design with a 12" x 12" x ¼ inch depression milled out of the 16" x 16" x ½" aluminum plate was chosen instead that requires roughly half of the amount of the oil needed previously which also addressed the issues of inlet/outlet integrity (Figure 3.16). The new design

dispensed with one of the polycarbonate cover plates so that the associated problem with the polycarbonate plate was cut in half.

Figure 3.16: low capacity sand pack

3.2 METHODS

3.2.1 Dry packing vs. wet packing

Sand packs were initially packed in slurry form with a resulting porosity of about 60% with well-sieved 30 mesh kaolinite. Similar sized kaolinite dry packing resulted in a sand pack with 56% porosity. Due to the lower porosity in the dry packing method as well as another issue of initial saturation discussed later, dry packing was chosen to be the method to be followed.

3.2.2 Methods to reduce initial water saturation of sand pack

Initially the sand pack was first vacuumed and then flooded with reservoir brine followed by flooding with oil to establish initial water saturation before aging. This method resulted in >30% initial water saturation which yielded flooding results that show no low salinity improvement. In the literature there are cases of unsuccessful low salinity floods attributed to reservoir already at an ideal wet state, so low salinity improvement from change in wettability was not possible. It was realized that a method of lowering the water saturation is needed in order to produce a sand pack that upon aging would reached a mixed wet if not oil wet state.

Various methods of artificially lowering the water saturation were tried out. Initially water saturation of kaolinite cristobalite sand was lowered by spinning in a centrifuge at 5000 rpm. This method though effective, was slow and tedious. The drying method of leaving the sands in high temperature oven was tried out, but the results were mixed since the salinity of the sands was increased to unknown level. Finally, a method involving wicking by use of paper towels is chosen because of its comparative ease and faster turn-around time. The sands that were immersed in reservoir brine overnight had the excess brine dump out. The wet sands were then spooned out and lay on many layers of extra adsorbent Bounty kitchen towels. As the towels got wet it was replaced until the majority of the brine were adsorbed away from the sands. The resulting sands were then spread as evenly as possible on a flat surface covered with several layers of the same adsorbent paper towels and left overnight. Once the sands had been air-dried thus on paper towels, the sands were collected and put into a jar and left to equilibrate for a day. The resulting sand had between 4-6% by weight of residual brine left at the initially salt concentration.

3.2.3 Experimental Set Up

The 1 D and 2D sand pack experiment has the following set up shown in Figure 3.17 and 3.18.

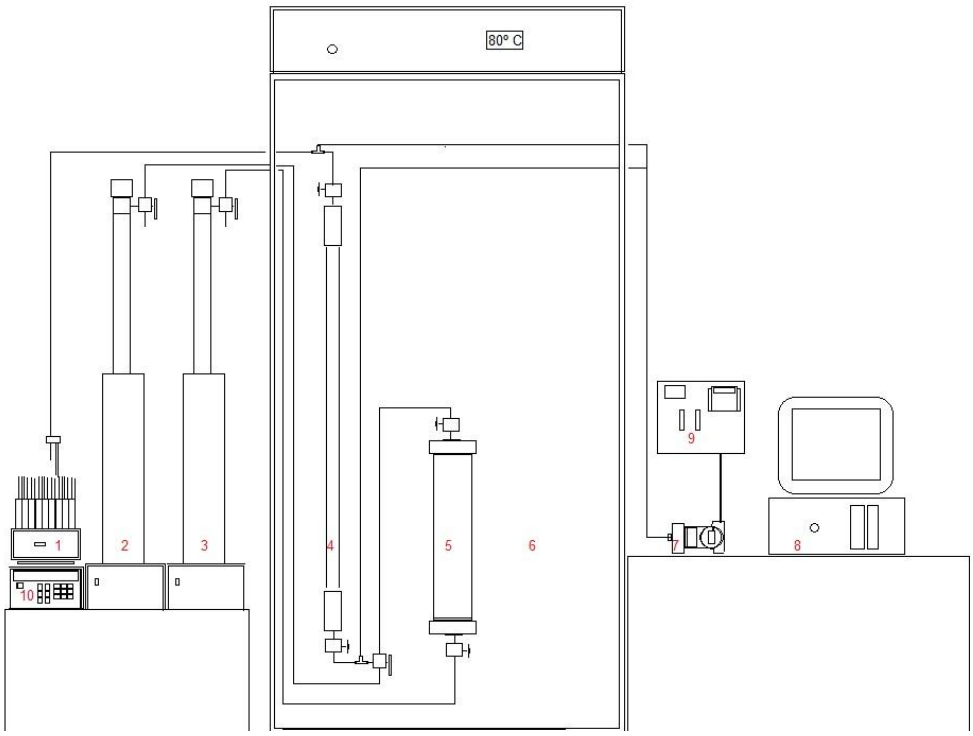

Figure 3.17: Set up. 1. Fraction collector 2. Brine pump 3. Oil pump 4. Sand pack 5. Piston cylinder 6. Oven at 80 degree C 7. Rosemount pressure transducer 8. LabView data acquisition user interface 9. NI USB 6008 12 bit, 10 kS/s Multifunctional DAQ and Omega Process Power Pack

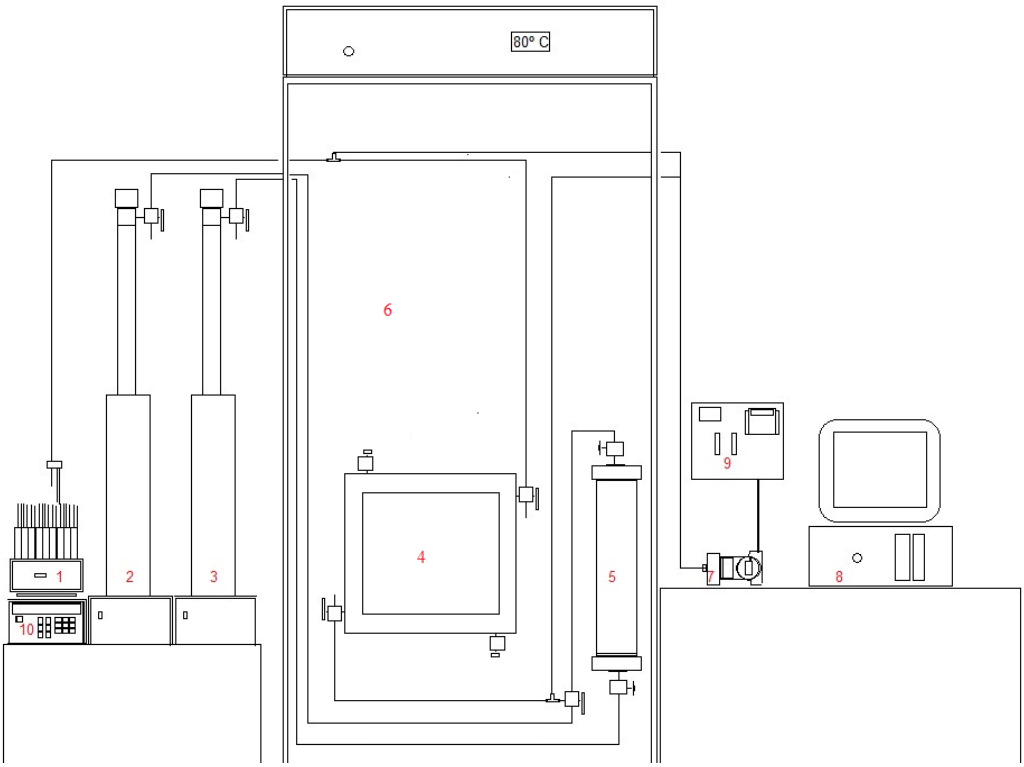

Figure 3.18 : Set up. 1. Fraction collector 2. Brine pump 3. Oil pump 4. Sand pack 5. Piston cylinder 6. Oven at 80 degree C 7. Rosemount pressure transducer 8. LabView data acquisition user interface 9. NI USB 6008 12 bit, 10 kS/s Multifunctional DAQ and Omega Process Power Pack

3.2.4 Data Analysis

3.2.4.1. Eluant analysis using Dionex Ion Chromatograph

The ion composition of the eluant offers a vital clue to infer what's going on at the rock surface. Ion Chromatograph therefore is a valuable tool to help understand the surface chemistry going on at the rock/oil/brine interface. Eluants from the floods were analyzed for cation composition. Dionex Ion Chromatograph is shown in Figure 3.19.

Figure 3.19: Dionex Ion Chromatograph 3000

3.2.4.2 Viscosity analysis

Viscosity of the fluid phase including crude oil and brine are analyzed by TA Rheometer (Figure 3.20). Viscosity measurement at reservoir temperature is possible with this instrument. The viscosity of the crude oil and brine were measured at 80 degree C using this instrument.

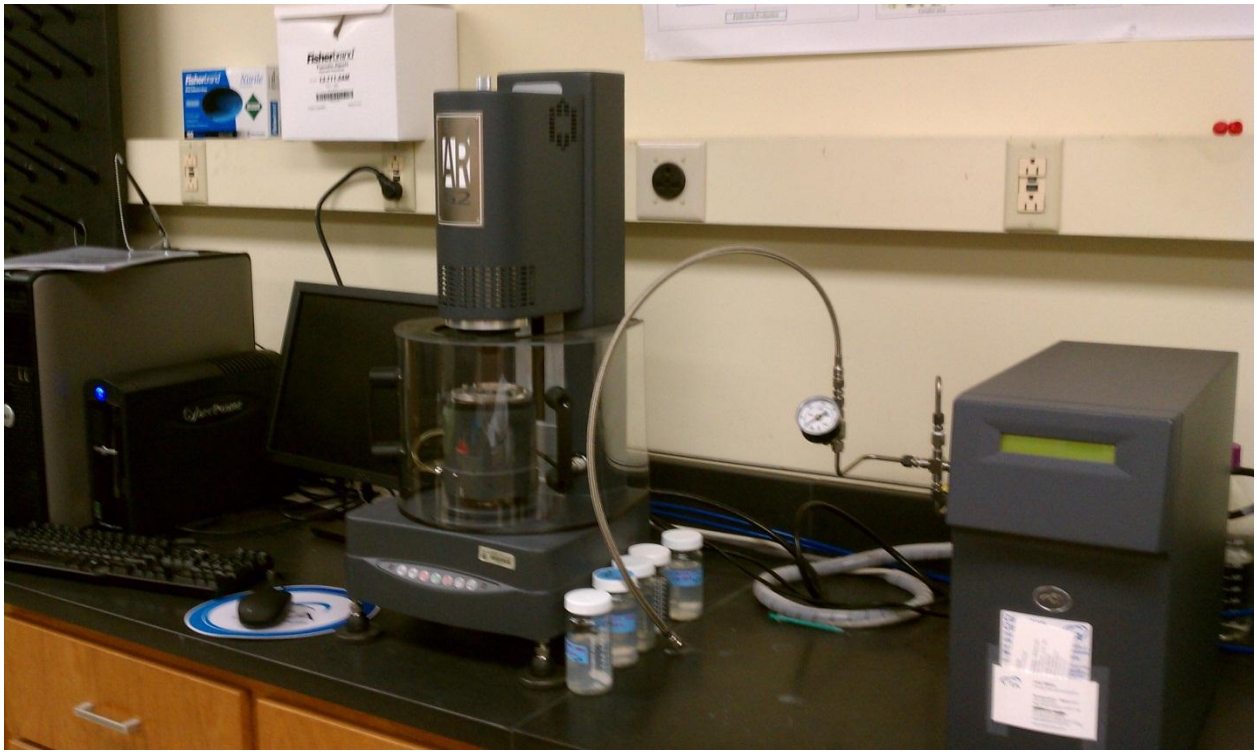

Figure 3.20: TA rheometer.

3.2.5 Fraction analysis

A slight different set up for oil fraction analysis was used toward the end of this project to minimize error. Gross errors in earlier experiments on eluent analysis caused ultimate recovery to be higher than 100 percent. In an attempt to correct this error, 25 ml graduated cylinder with slightly larger outer diameter was used rather than the more common 10 mL glass tubes. Using the bigger graduated cylinder can allow for fraction volume of up to 30 mL which enable thicker oil eluant fractions in each sample, allowing easier estimation and lessening waste of oil. It is fully realized, however, that the increased accuracy of oil recovery comes at the expense of sacrificing the accuracy of ion analysis. Given that the trend for oil recovery usually entails heavier oil fractions in the

beginning which coincide with the most interesting ion exchange data, a two-step fraction collection scheme is used which entailed smaller fraction collection in the front to have finer ion exchange characterization in the immediate aftermath of brine breakthrough and the 25 ml graduated cylinder collections one PV after breakthrough. Equation for analyzing the amount of oil has been standardized using an equation of a simplified disk (Figure 3.21).

$$Volume_{oil} = \frac{(D_1^2 - D_2^2)\pi}{8} h$$

Volume of oil is in ml. D_2 is the diameter of the brine circle as shown in Figure in cm. D_1 is the diameter of the graduated cylinder which is 1.552 cm. The width of D2 is measured with a ruled paper.

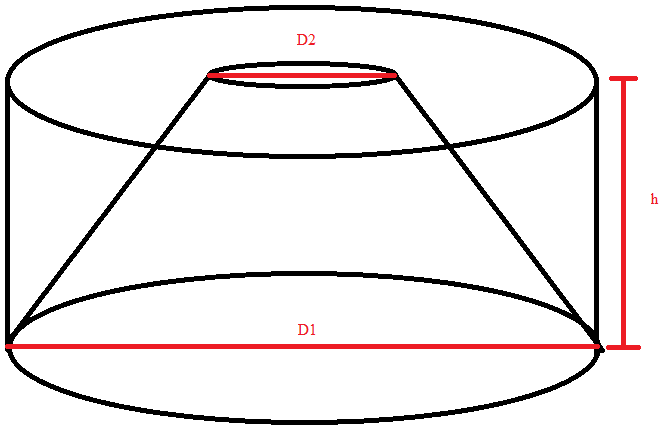

Figure 3.21: Approximation of oil in graduated cylinder

Chapter 4: Results and Discussions

4.1 Qualitative Experiments

Wetting experiments were conducted to find oil/rock/brine system that will produce oil wettability in the presence of high salinity brine and water-wettability in the presence of low salinity brine. The first experiments show a 1 ml oil-aged kaolinite-sand bed exposed to 5 bed volumes of HS or LS brine (Figure 4.1). The results showed that The LS brine showed a thicker oil recovery than the HS case. The HS case shows a clumpier sand/oil structure indicating a more mix-wet state. The LS case shows a more discretized sand/oil structure indicating a comparatively more water-wet state.

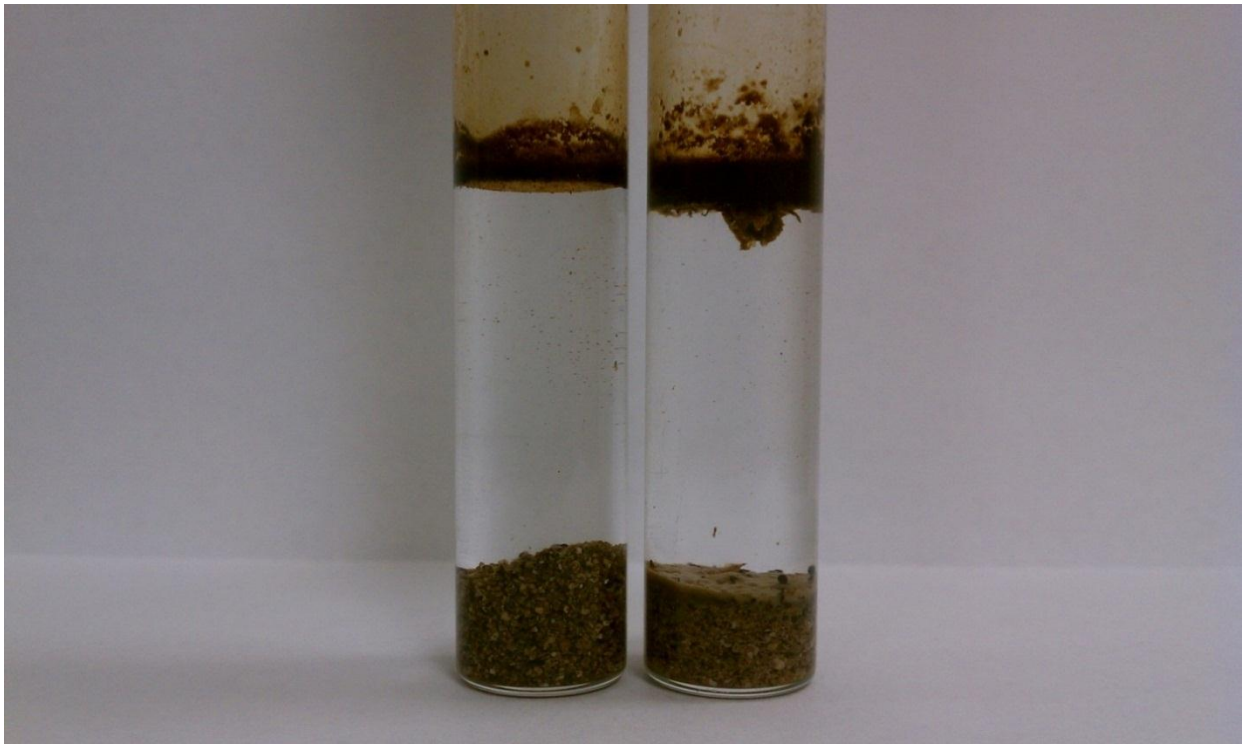

Figure 4.1: HS vs. LS qualitative experiments

4.2 1D Flooding

The 1D flooding experiments were conducted with two 1 foot long sand packs. The sand packs were packed with the sands prepared as detailed in the methods section with a water weight percentage of 4%. The two columns were packed to be as close to each other as possible with column 1and 2 having pore volume of 24.3 and 23.5 mL, respectively, with corresponding porosity of 52 and 51%. Column 1 is used for HS flooding and column 2 is used for LS flooding. A similar sand pack is flooded with brine to get a brine absolute permeability of 19 Darcy and this is taken as the absolute permeability for both columns. Column 1 and column 2 both have the same initial water saturation of 8% and an initial oil saturation of 92%. Column 1 and 2 were both aged at 80 degree C and flooded respectively for HS and LS flood. Before water flood, both columns were flooded with 2 PV of oil.

Figure 4.2 shows the results of the pressure data and oil recovery of the HS and LS floods. Brine breaks through at 0.47 PV in the case of the high salinity waterflood. The final recovery is about 0.62 PV in about 4.3 PV of waterflood. The low salinity waterflood was also a secondary flood. The brine breakthrough for LS case occurred earlier than the HS case at roughly 0.36 pore volume whereas the HS case was at 0.47 pore volume. The LS flood resulted in a 15% higher oil recovery (about 0.77 PV) than the HS flood after roughly 4.3 pore volume of flooding. The residual oil saturation was 31% in the LS flood compared to 14% in the case of the HS flood. The higher oil recovery for the low salinity case seemed to match the literature trend, falling within the 2-40% additional oil recovery range. Because of the relative short length of the sand pack

and the very high porosity nature of the packing material, the pressure drops for both floods were very low. The pressure measurement was noisy and not very accurate. The pressure drop in the HS flood was a little higher than that in the LS flood, but both showed a decreasing pressure trend after the breakthrough. Thus there was no evidence of severe fine migration and plugging in this sand pack.

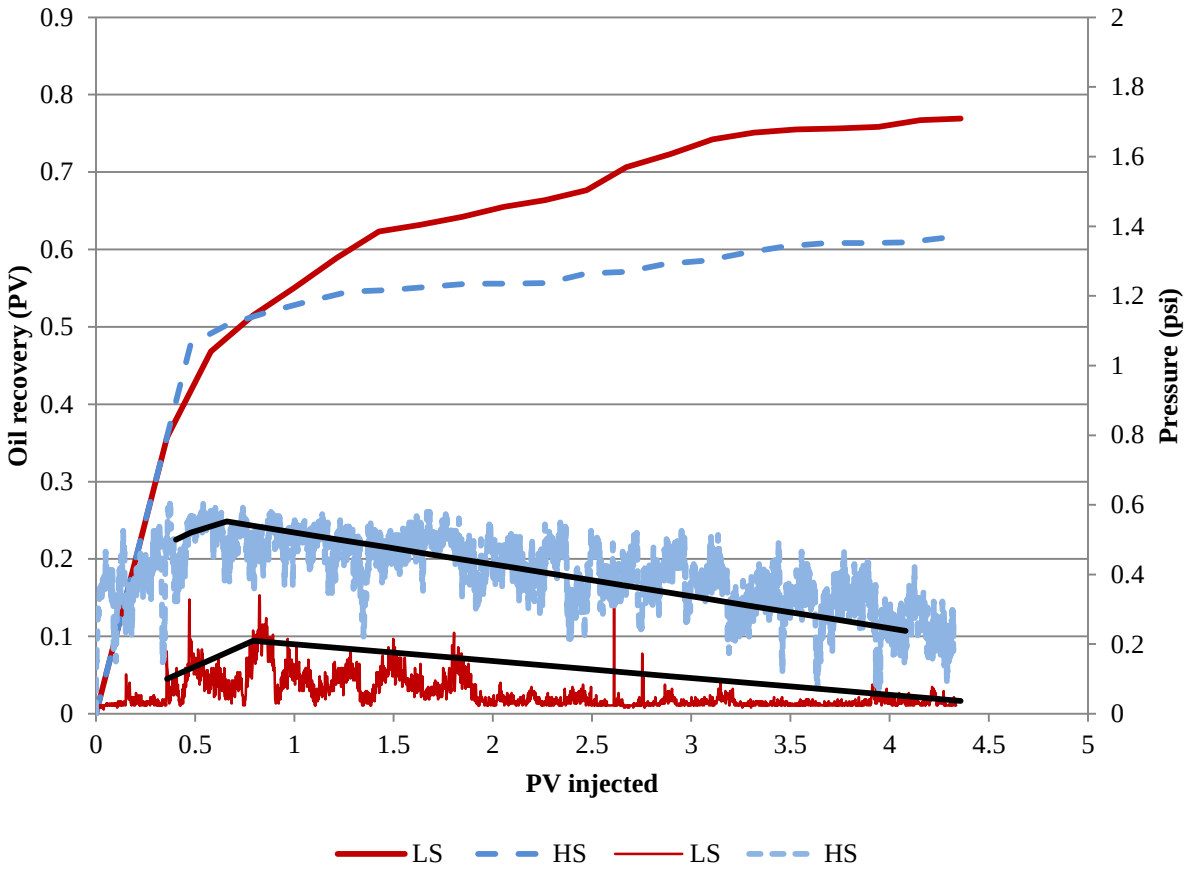

Figure 4.2 HS and LS flooding oil recovery and pressure data

For low salinity flooding, there is often literature evidence of increasing pH during the flooding. Despite a few contrary evidence, for the bulk of the literature on low salinity flooding, an associated 1 to 2 point increase in pH is often reported. The oil recovery and

pH are shown in the Figure 4.3. The initial pH of the HS and LS brine are 6.2 and 6.3, respectively. The packing material turns both the HS and LS brine acidic. The decrease in pH for both brines during the aging process is roughly 1.5. During the waterflood, the pH increases to 6.2 and 5.8, respectively. The explanation found in literature that can potentially explain this is the possible hydroxylation of the aluminum in kaolinite.

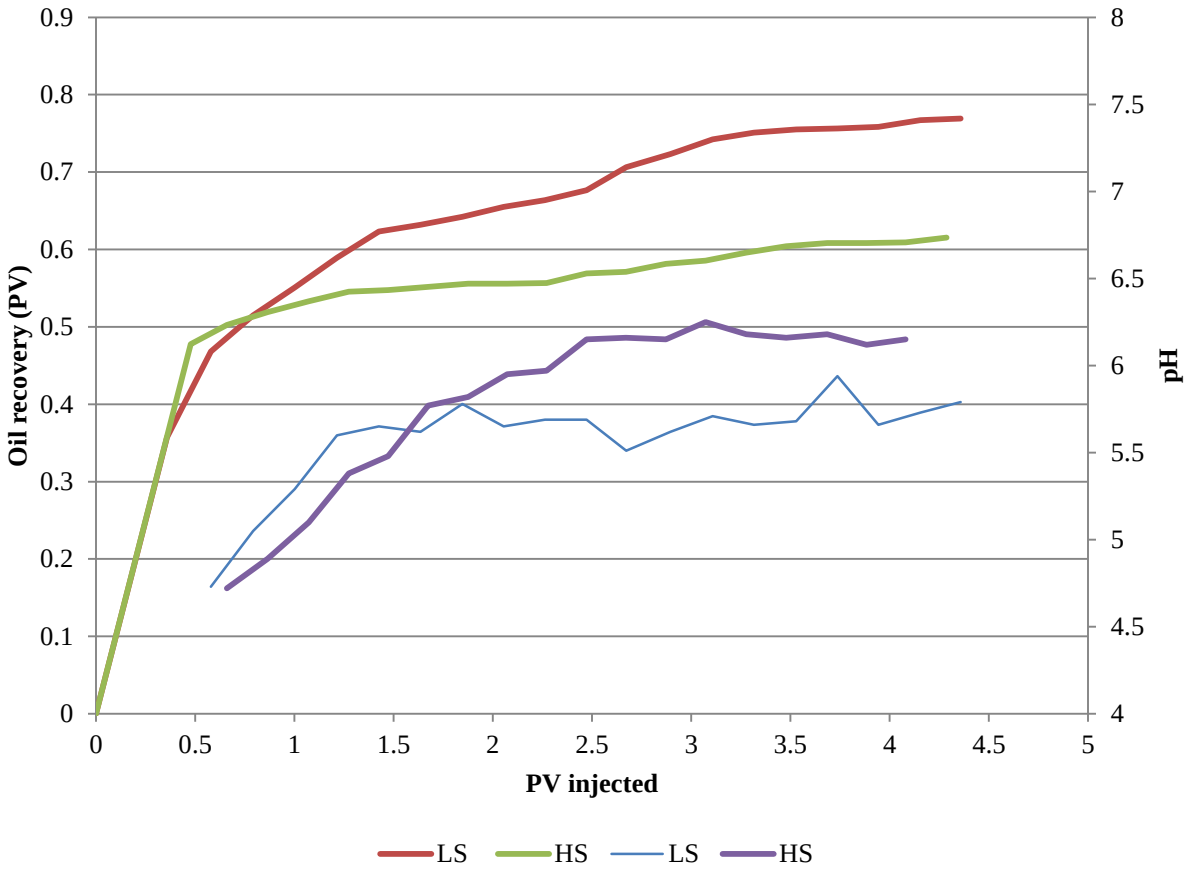

Figure 4.3: HS and LS flood oil recovery and pH vs. pore volume injected

While the decrease in pH during aging is puzzling, the increase in pH is a good representation of what is going on in the reservoir. Typically, the reservoirs contain a certain amount of CO_2 and H_2S which makes the reservoir acidic around pH 5. It is worthwhile to note that the pH for both HS and LS started out at 4.7 but ended with HS

back to its starting brine pH of 6.2 and LS still 0.5 pH point lower than its starting brine pH of 6.3. Since the pH of both brine started out 4.7 and ended within 0.4 pH point apart, this suggests that the solid surface plays an important role. It is important to note that despite the rise in pH for both cases, the rise in pH was actually higher for HS case. Figure 4.4 shows the plot of the cation concentrations for HS flood as a function of pore volume. The starting concentrations of HS brine, taken from IC (ion chromatograph) bottle, and taken from pump are shown in Table 4.1.

	HS brine	IC_pump	IC_HS brine bottle
Na	7867	7612	7357
K	10489	8475	8328
Mg	5120	6574	5861
Ca	7226	8688	8518

Table 4.1: HS brine concentration

These concentrations are somewhat different than the actual amount when the brine was first made, suggesting that there was a pipetting error compounded by the one hundred fold dilution of all HS samples in order to be run on the ion chromatograph. In the event of pipetting error, since all the samples are diluted similarly at one hundred fold (the HS injection brine from the pump included), the results should still be comparable. After four pore volumes of HS flooding, mass balance shows that all four cations are less than the injection concentration, suggesting that cations are continuously being adsorbed on the kaolinite.

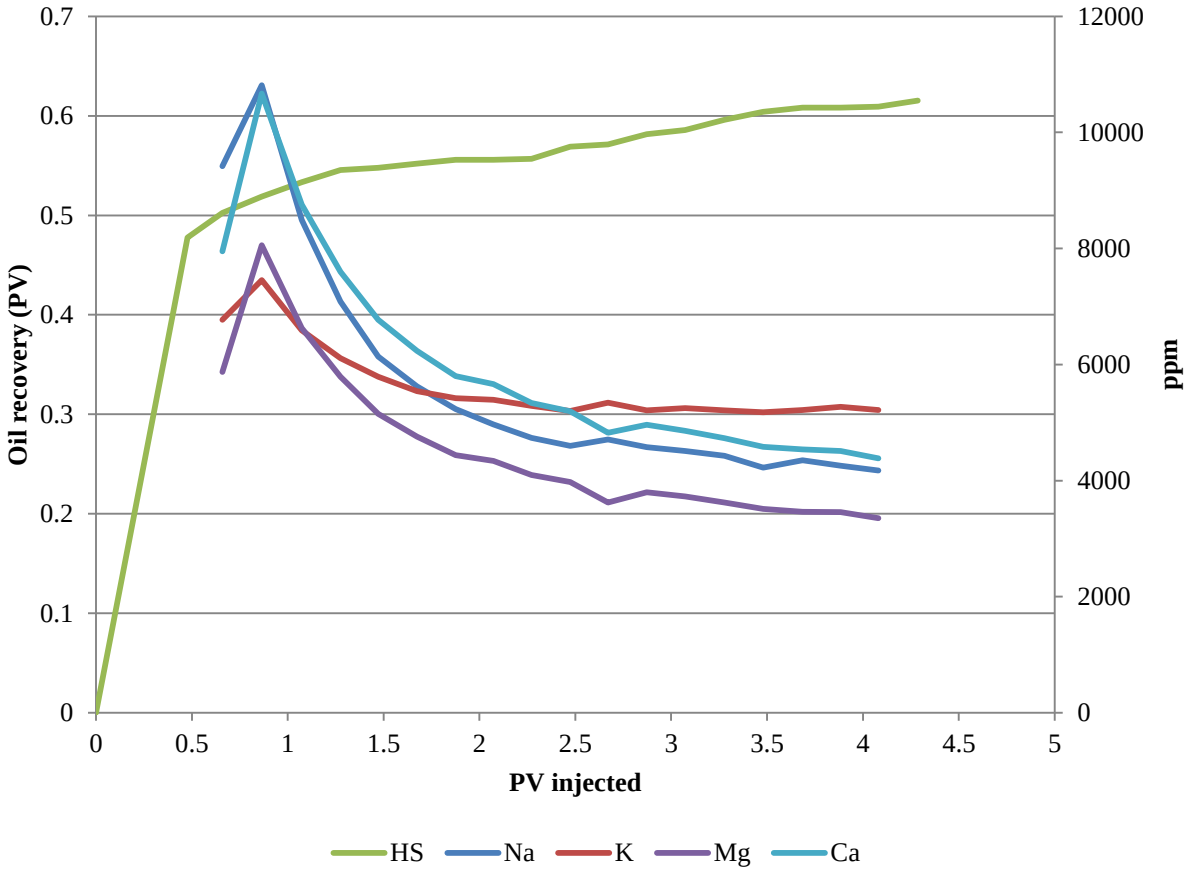

Figure 4.4: HS flood oil recovery and cation concentration vs. pore volume injected.

Figure 4.5 shows the LS effluent cation analysis as a function of pore volumes flooded. The LS brine initially was made to have 393 ppm of Na^{+} only. Due to the contamination from the pump there are K^{+}, Mg^{++}, and Ca^{++} in the LS brine even though they are not made with these elements. The LS brine composition from the pump as per ion chromatograph analysis is 226, 38, 18, and 26 ppm of Na, K, Mg, and Ca, respectively. The Na concentration is lowered than expected. This is attributed to operator's error in making the brine.

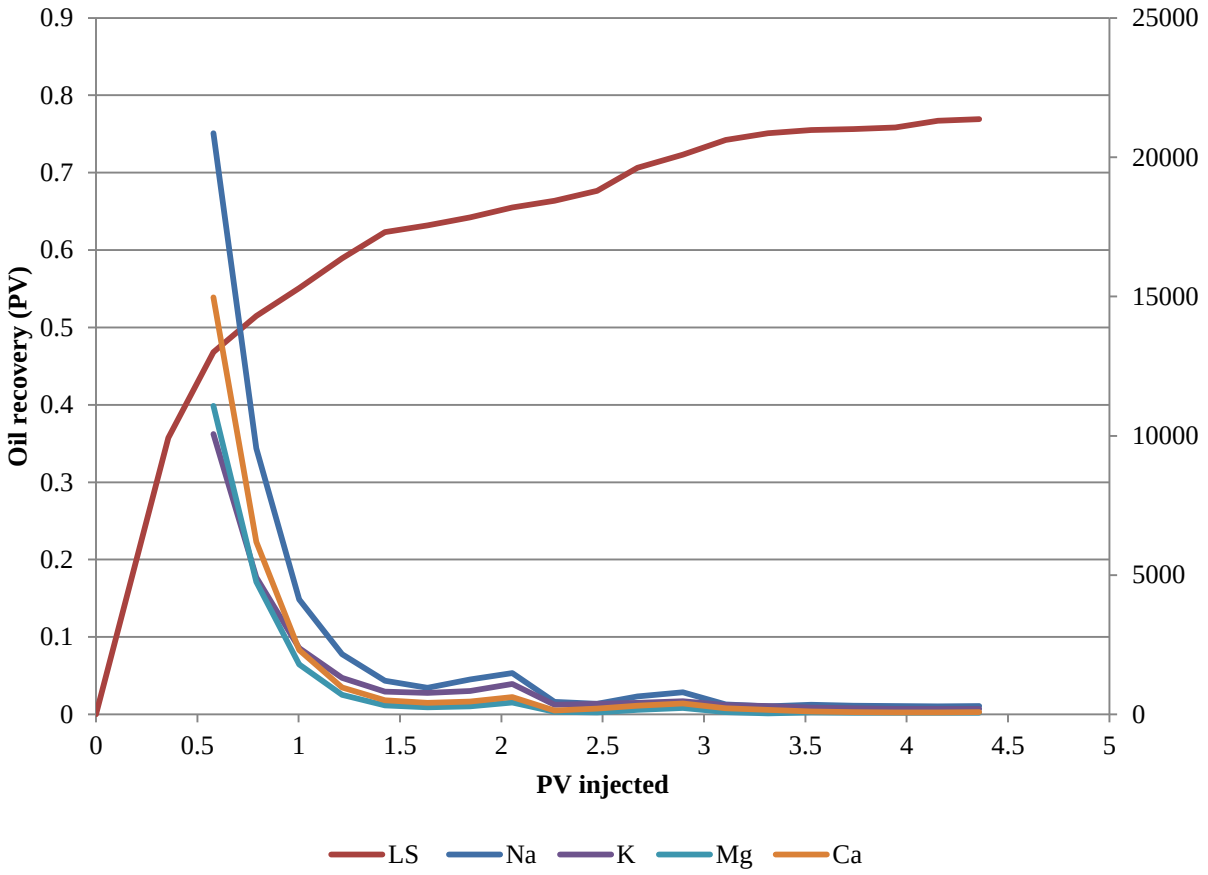

Figure 4.5: LS flood oil recovery and cation concentration vs. pore volume injected.

By comparing Figure 4.4 and 4.5, it is apparent that in the beginning of LS flood, the initial concentration of all of the cation appears to be higher than the HS case. The cation concentrations are listed in Table 4.2.

	Na	K	Mg	Ca
HS	9415	6769	5870	7951
LS	20856	10069	11079	14967

Table 4.2: Breakthrough cation concentrations in HS and LS floods

Since both columns for LS and HS flooding are packed with the same sand at the same water saturation, the higher cation from the LS sample cannot have come from anywhere else except the rock surface. The LS brine simply does not have this high cation concentration (despite potential contamination). This table points out that LS floods displace much more of the adsorbed cations on the rock surface. This is an important evidence of the extent of cation exchange happening during the LS flood and gives a clue of its role in the underlying mechanism. Based on Table 4.2 and the Figures 4.4 and 4.5, cations are apparently adsorbing on kaolinite during HS flood and desorbing from kaolinite during LS flood. In other words, the clay during HS flood is becoming more cationic and during LS flood is becoming more anionic.

Figure 4.6 shows the relative permeability curves of the HS and LS floods. The relative permeability curves are only approximate because the pressure drop data had a lot of fluctuations. The HS relative permeability curves appear more water wet than the LS relative permeability curves. At higher water saturations, oil relative permeability is higher for the LS flood. The oil flows when water saturation is 85% for the LS case, whereas for the HS case the oil stops flowing at around 70% water saturation, indicating that the residual oil saturation dropped roughly 15% because of low salinity. This result

agrees well with the published literature. The other observation that can be made from Figure 4.6 is that the oil relative permeability is approximately twice as for HS compared to LS at low water saturation, suggesting that oil flows a lot better at low water saturation for the LS case.

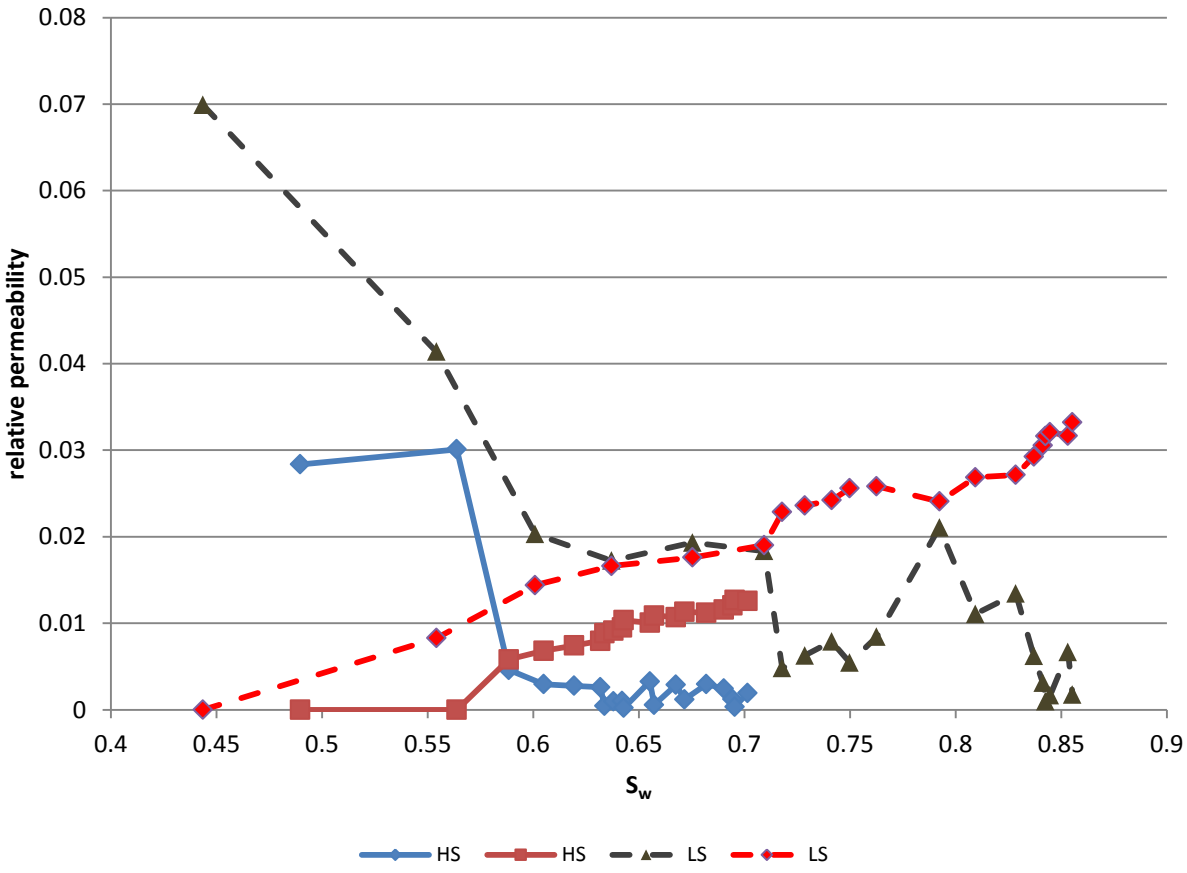

Figure 4.6: Relative permeability of HS and LS flood

2D Sand Pack Flooding

The 2D sand packs were packed with the same packing material as the 1D experiments, injected with oil, and aged for two weeks at 80 degree C. The properties of the 2D sand pack for LS and HS flood are roughly the same at 430 mL pore volume and 50% porosity. The 2D sand pack used for LS flood developed a blockage and had to be taken apart and wet-packed. Since the dimension of the two sand packs are the same, the pore volume and porosity of the first sand pack was assumed to be the same as the second sand pack used for HS flood.

The oil recovery and pressure drop of the 2D HS flood are shown in Figure 4.7. The recovery is approximately 28% after one pore volume of HS flooding.

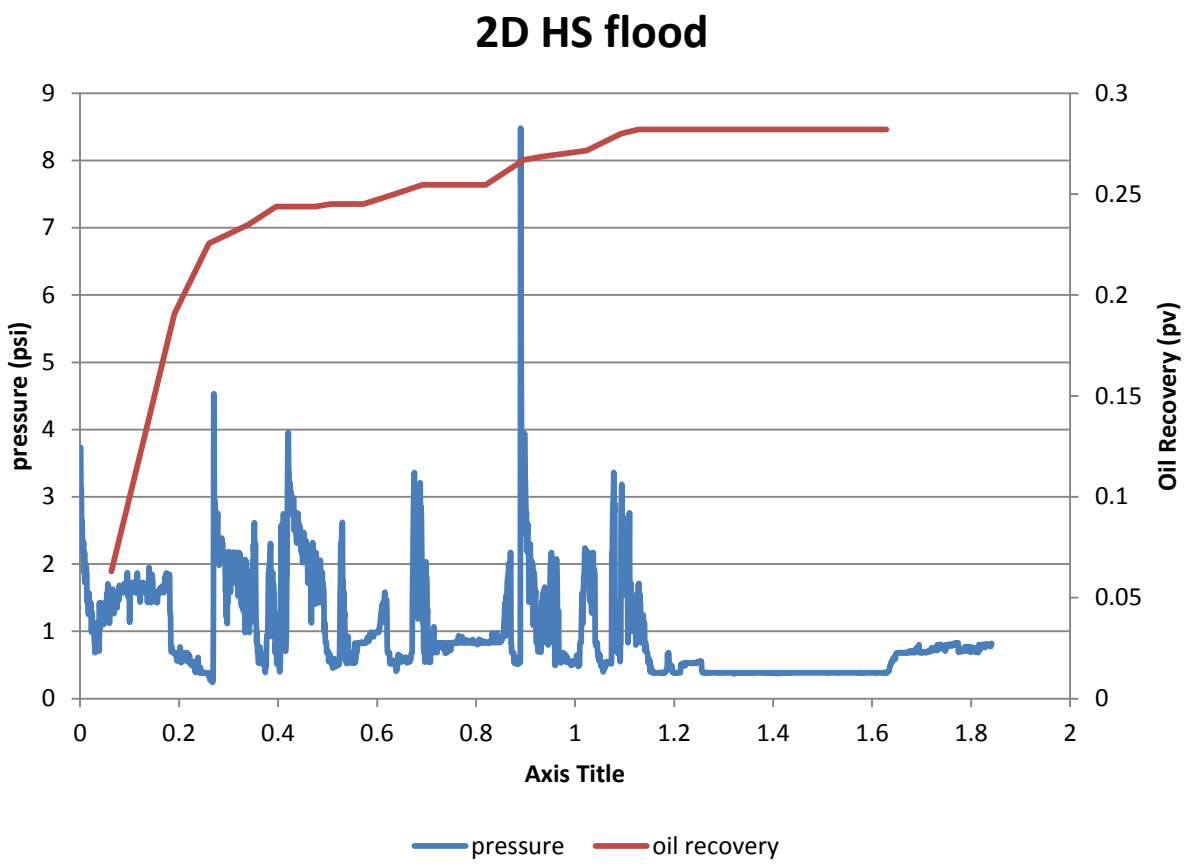

Figure 4.7: 2D HS flooding

The digital recording of the flood fronts is shown in Figure 4.8. The recording were done using a Swann all-purpose security camera with 540 Line 1/3" Sony "SuperHAD" high-resolution video sensor. The images were captured and stored by DigiVue PCI BASED A/V DVR system on a Dell PC. The images are laid out in 1 hour increments. The fluid is injected at the bottom right hand corner and produced diagonally across at the top left hand corner. There is a missing image on the first row due to file corruption which is left blank. The flood front is hard to see for the HS flood case because the rock is still very much oil-wet.

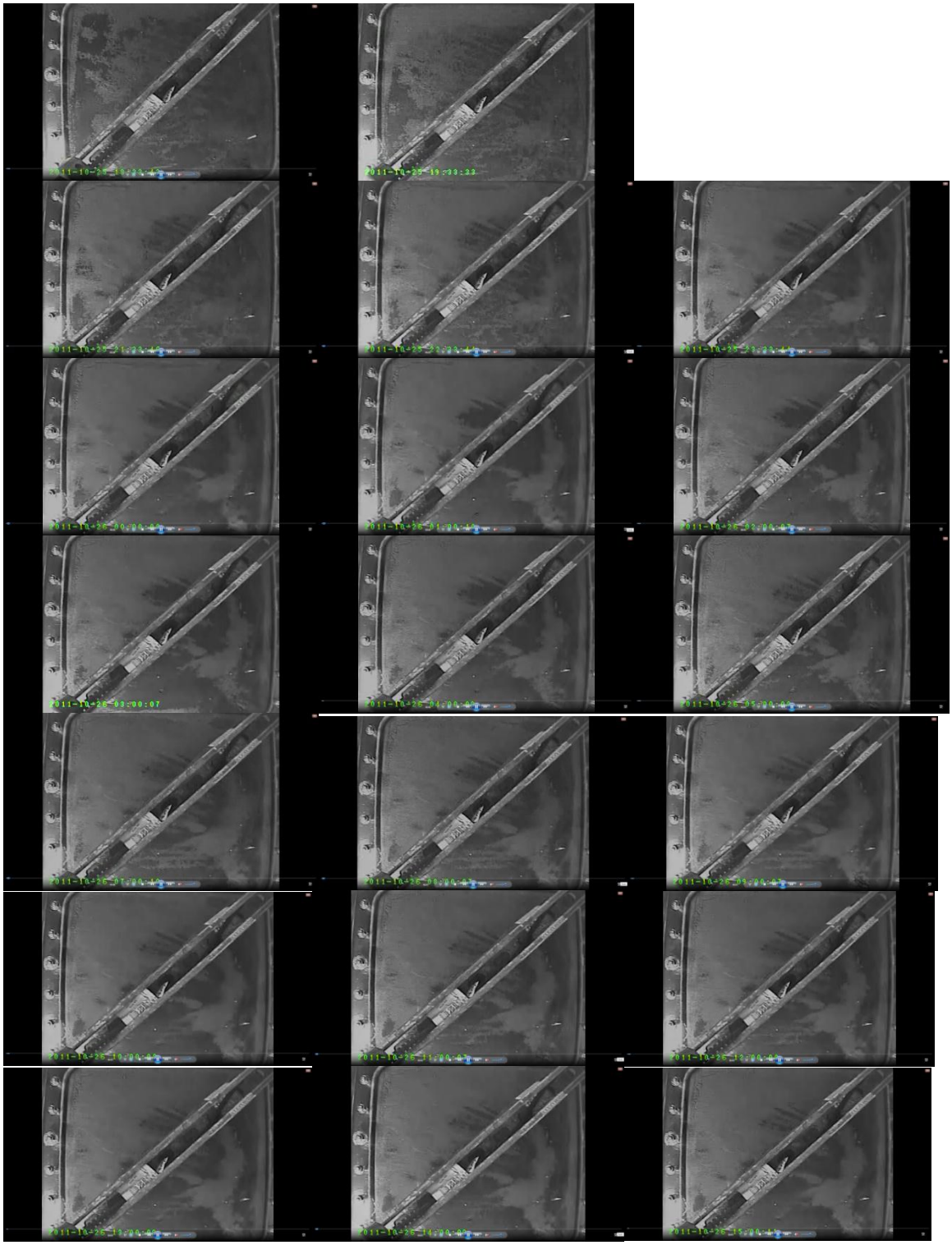

Figure 4.8: 2D HS flood

Figure 4.8 (continued): 2D HS flood

For the 2D LS flood, the sand pack developed a leak after the breakthrough and the oil recovery was 33%. Figure 4.9 shows the movement of the floor front for the 2D LS flood. Qualitatively speaking, the 2D LS flood seemed to have a much more visible flood front. On inspection, the sands in the 2D LS flood looked a lot whiter than that of HS flood suggesting a much more water wet state.

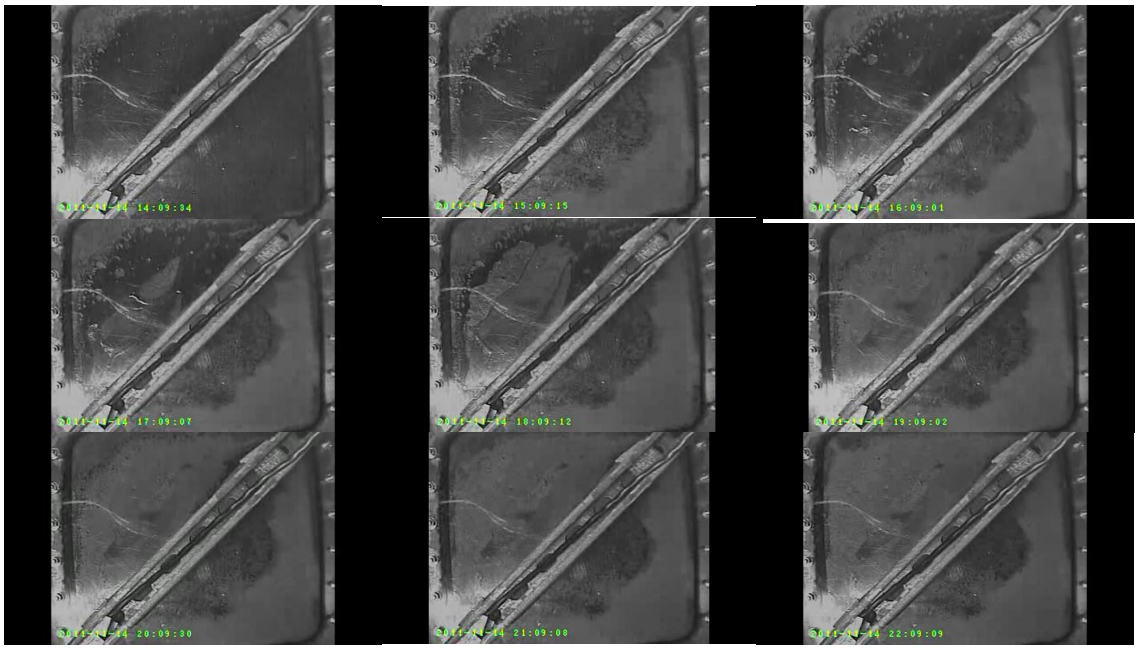

Figure 4.9: 2D LS flood

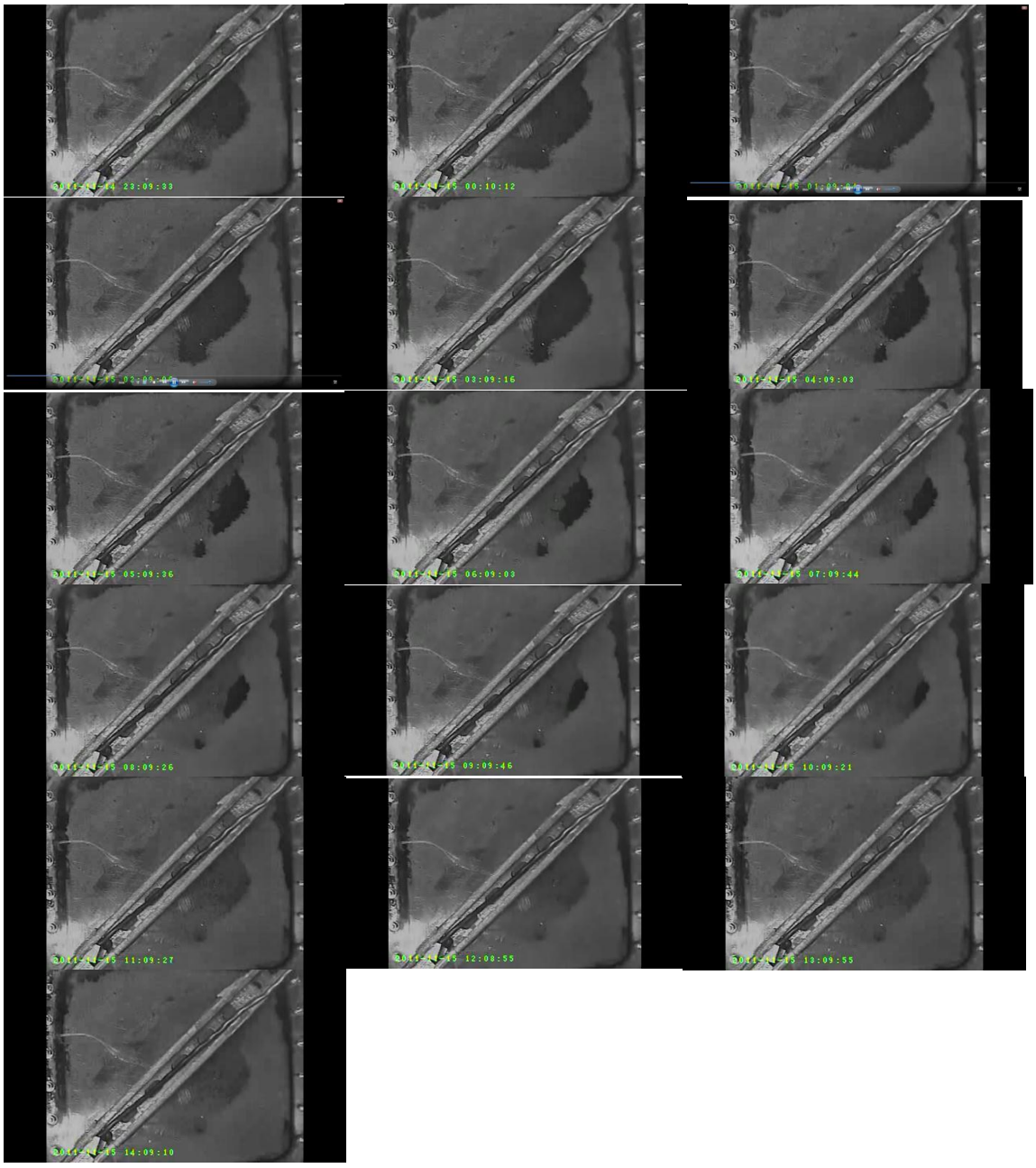

Figure 4.9 (continued): 2D LS flood

The 2D LS flood appeared to be pushing the oil out from the sides first. It appears to be more unstable, possibly due to the low mobility ratio across the low salinity front discussed in the introduction. The images for 2D LS flood showed a better sweep of the

Discussion of Driving Mechanism

To understand low salinity waterflooding, the interaction between rock, brine, and crude oil must be studied. In this section, the results from this study as well as from published literature will be discussed to arrive at a most likely underlying mechanism.

The crude oil has three basic fractions: basic, acidic, and paraffin. The interactions they can have with the rock surface are reported to be cation exchange, ligand bridging, and Van Der Waals interaction (Figure 4.10). The mechanism by which acidic fractions can bind to the surface proposed by Austad et al. (2010) is also included in Figure 4.10.

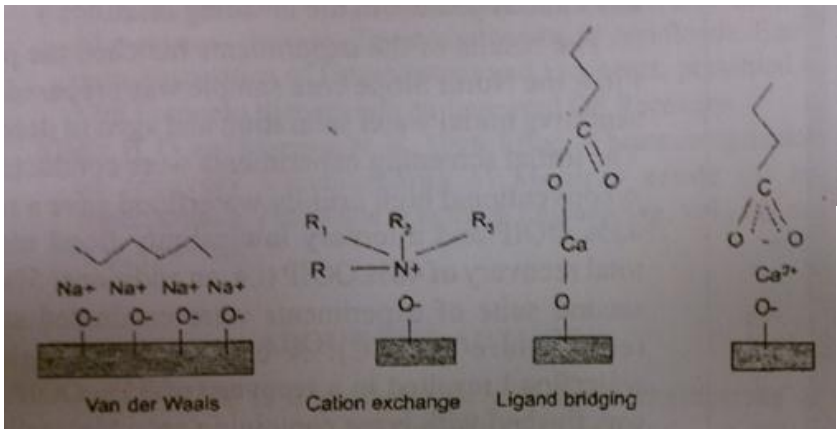

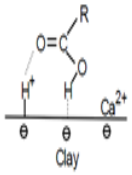

H-bonding

Figure 4.10: Adsorption mechanisms (Lager 2008, Austad 2010)

Each oil is different in terms of the composition of paraffinic, basic, and acidic fractions; therefore it is expected that each oil will interact with rock and brine by different mechanisms. But some generalizations can be made from the abundance of each respective fraction. The crude oil, for the most part is paraffinic, composed of pure hydrophobic hydrocarbon chains. The polar components that are responsible for interaction with the rock surface via the stronger interactions (cation exchange, H-bonding, cation bridge) are mainly the naphthenic acids and pyridines functionalities both found in the heavy-fraction of the crude oil. The mechanisms listed in Figure 4.10 do not include hydrophobic interactions between the nonpolar paraffin themselves. Though hydrophobic interactions do not directly interact with the surface, they do help by precipitating the crude oil toward the surface to facilitate adsorption by Van der Waals interaction (Figure 4.11).

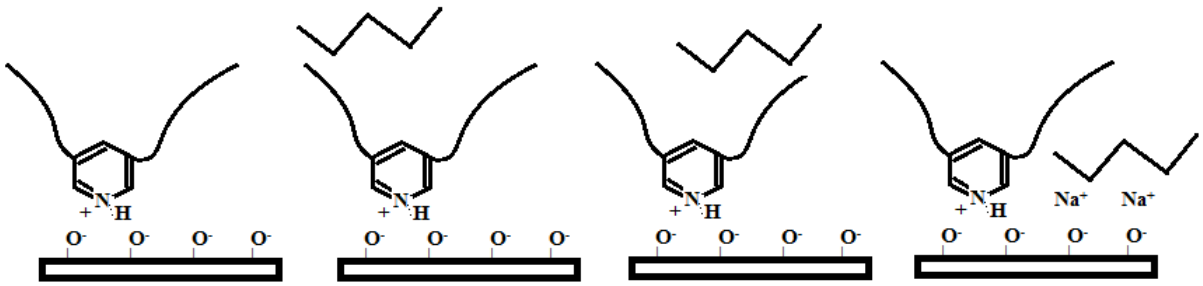

Figure 4.11: Hydrophobic interactions for precipitation of crude on surface.

Very often in the sandstone reservoir at high temperature, the base number is significantly higher than the acidic numbers. By the relative abundance of each fraction, the relative ratio of interactions can be thought of in terms of the following order:

Van Der Waals (paraffin) > cation exchange (basic) > cation-bridge (acidic fractions)

Figure 4.12 shows a desorption profile of two similar two inch columns packed with ~ 2.5 ml of 50 mesh kaolinite sand flooded with ~70 PV of 50,000 ppm Ca solution. The two plots show results of flooding with 50000 ppm Na and 1000 ppm NaCl solutions.

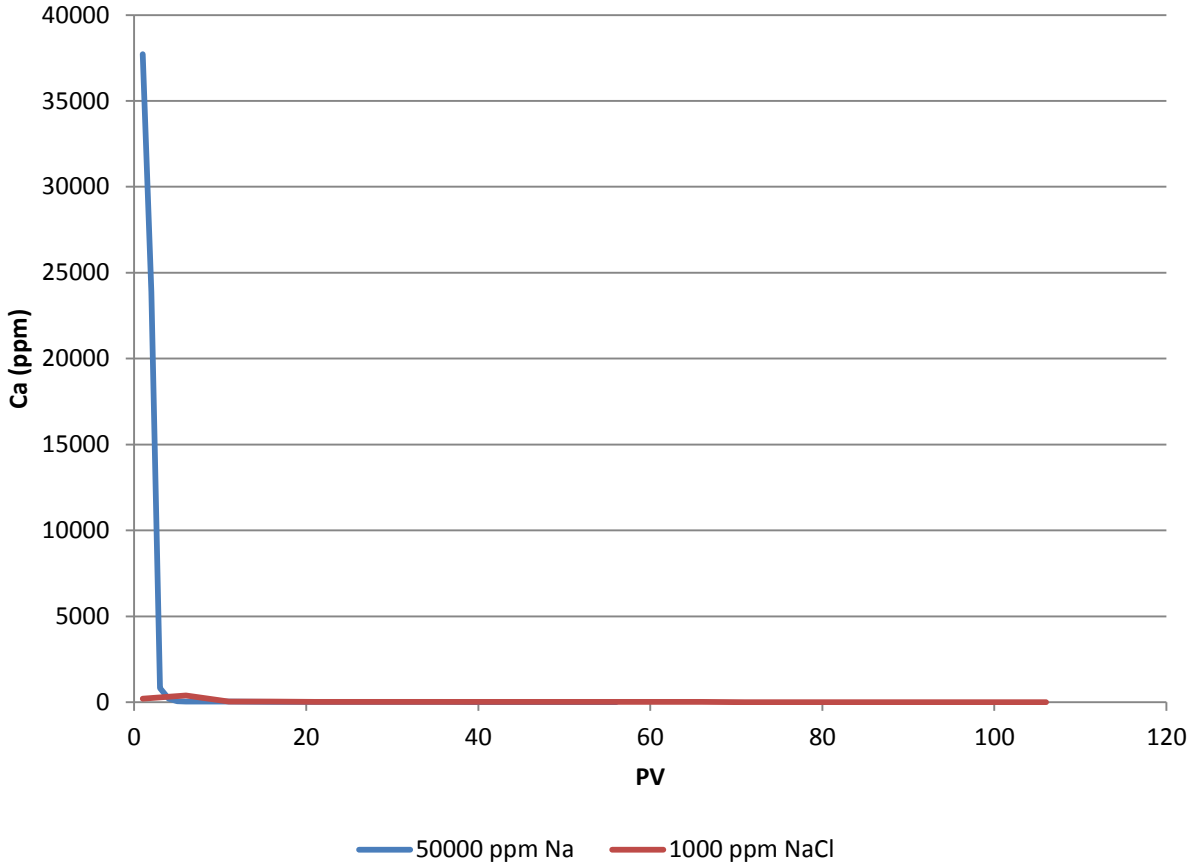

Figure 4.12: Desorption profile of 2.5 mL kaolinite columns saturated with Ca.

From Figure 4.12, it is seen that the calcium desorption from the surface is slow under low salinity conditions, whereas the desorption of calcium under 50000 ppm Na flooding conditions is rapid. Since the two columns are similar in total cation capacity, it is apparent that a great majority of the calcium adsorbed did not come off after 100 pore

volume of 1000 ppm NaCl flooding. The conclusion drawn from this is that calcium desorption at LS condition is a very slow process.

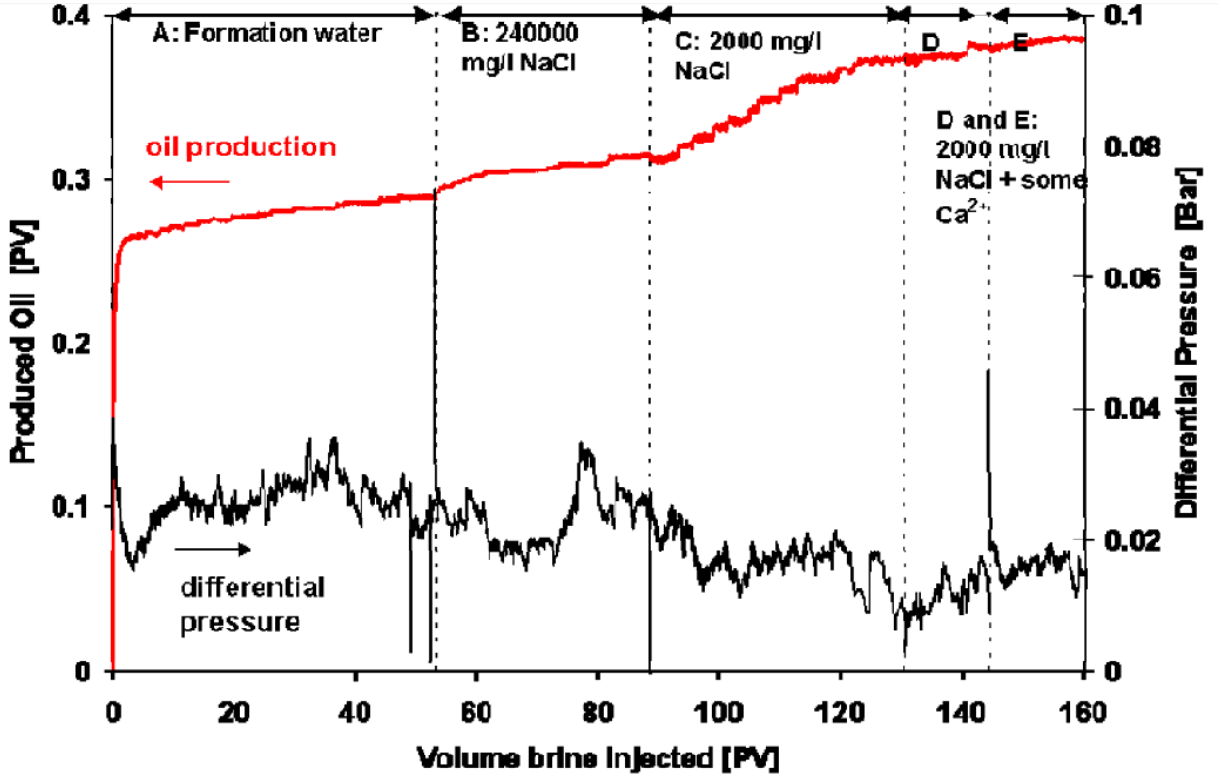

Figure 4.13: Oil recovery for core flood (Ligthelm 2009)

Given that the acidic components under reservoir conditions are smaller than the basic fractions, Figure 4.13 give an example of what the acidic fraction percentage could be in the total oil recovery. Phase A is a conventional flood using formation brine which has the formula listed in Table 4.2. The relative high divalent cation concentration is thought to reversed some of the desorption of cation-bridge bound hydrocarbon by the high sodium concentration. Phase B is a pure high concentration sodium flood which would knock out the remaining cation bridge bound hydrocarbons. Based on this plot, it is seen that ~0.03 pore volume of assumed cation-bridge bound oil is thus desorbed after the

conventional flood B, and assuming that the cation-bridge bound oil desorbed during phase A is no more than the percentage desorbed in the following phase B of 240000 ppm NaCl, the cation-bridge bound oil should therefore be no more than .06 pore volumes. Under the low salinity condition, the combination of the slow kinetics of calcium desorption and the relative small fraction of cation-bridge bound oil suggest that cation- bridge bound oil does not contribute much to the recovery improvement during low salinity flood.

(Synthetic) Formation Water	mg/l	mMol/l	meq/l	contribution to I, Mol/l
Na^+	84288	3666	3666	1.83
Ca^{2+}	6800	170	339	0.34
Mg^{2+}	1215	50	100	0.10
Cl^-	145556	4106	-4106	2.05
TDS	**237859**			
I(Mol/l)				**4.33**
N(meq/l)			**4106**	

Table 4.3: Formation brine (Ligthelm 2009)

The acidic fraction adsorption mechanism by H-bond proposed by Austad shown in Figure 4.10 is thought to have a stable analogue in the dimeric complex of carboxylic acid. His proposed mechanism requires a captured proton on the surface to interact with the electron-rich carbonyl oxygen. Given that the proton concentration at the reservoir pH of 4-5 (0.1-0.01 mM) is 2-4 order of magnitude less than the cation concentration in Table 4.3, this type of bond is probably a lot fewer than the cation-bridge type. Based on the analysis so far, acidic fractions adsorption on kaolinite does not contribute much in the low salinity incremental oil.

The basic fractions adsorb on kaolinite via cation exchange. As calcium concentration decrease, adsorption increases for the basic fractions. In another word, LS conditions enhance adsorption of basic fractions. Figure 4.14 shows adsorption of quinoline (an analogue to the basic pyridine functionalities found in heavy fractions) on kaolinite. As calcium concentration decreases, competition from them for the active site on kaolinite diminishes, therefore the adsorption of the basic fractions increases. From this knowledge, the basic fractions do not contribute to the low salinity recovery improvement.

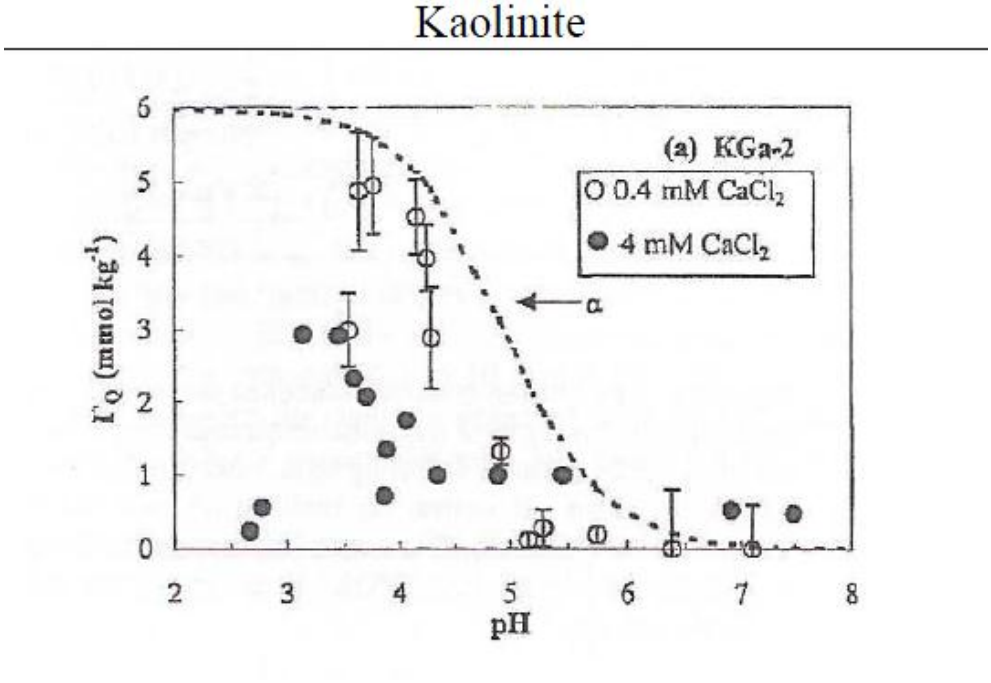

Figure 4.14: Quinoline adsorption on kaolinite (Austad 2010).

Van der Waals interactions are the most numerous interactions simply because paraffinic fractions make up a greater portion than the acidic and basic functionalities in the crude oil. Though the Van der Waals interaction is the weakest, by sheer quantity, it makes up

the bulk of the interaction between the crude oil and the rock surface. It is the only interaction that can account for the up to 40% improvement witnessed for some of the low salinity recovery results. The basic and acidic fractions simply do not have the large enough ratio in the crude make up to contribute to such a large recovery improvement. Lager et al. (2006) and Ligthelm et al. (2009) proposed the expansion of electric double layer as the driving mechanism for low salinity recovery improvement. Lee et al. later provided experimental measurement of the increased thickness of the double layer at low salinity conditions that serves as evidence of this phenomenon (2010). This study provided result in Table 4.2 that shows the extent of cation desorption during LS flood. The desorption of the surface bound cations (mainly sodium) that serve to bind the paraffinic fractions to the surface via Van der Waals interaction free the captured oil. This mechanism makes the main contribution to the low salinity oil recovery. The diffusion of the surface bound cations from cation-rich surface to cation-poor supernatant is the cause of the swelling of the electric double layer, not the effect. The concentration gradient between the surface and the supernatant is the driver for the passive diffusion of cations. This diffusion-driven cation exchange is the cause of the swelling of the electric double layer, and the low salinity recovery improvement.

Chapter 5: Conclusions

The effect of salinity on waterflood was studied in 1D and 2D clay-rich sand packs. The oil-aged clay-rich sand was oil-wet with the high salinity (HS) brine and turned slightly water-wet with the low salinity (LS) brine. LS water flooding gave an incremental oil recovery of 15% in 1D sand packs compared to the HS waterflooding. The oil relative permeability increased in the presence of the LS brine indicating a more water-wet state. The ion analysis of eluant showed a trend of cation adsorption during the HS flooding and cation desorption for the case of the LS flooding. The diffusion-driven cation exchange plays an important role in the wettability alteration. Multi-component ion exchange mechanism, originally offered by Lager (2006) can explain the oil-wettability due to oil bound by cation-bridging, but not the Van der Waals interaction-bound oil. The expansion of electric double layer proposed by Ligthelm (2009) and Lager (2006) has been confirmed by experiment (Lee 2010). This is proposed by them as the cause of the low salinity improvement. It is proposed in this study that the swelling of the electric double layer is the effect, and not the cause. The diffusion-driven cation exchange is believed to be the driving mechanism for low salinity water flooding.

The 2D study focused on capturing the movement of the water saturation fronts in transparent 2D sand packs via digital recordings. Low salinity flooding yielded higher oil recovery at breakthrough than the high salinity case. There was more areal bypassing in the case of low salinity flooding. The heterogeneity of the 2D sandpacks affected the waterfloods. Further studies are needed to reduce the heterogeneity of 2D sandpacks and conduct HS and LS waterfloods in these improved sand packs.

References

Agbalaka, C.C., Dandekar, A.Y., Patil, S.L., Khataniar, S., Hemsath, J. 2008. "Coreflooding Studies to Evaluate the Impact of Salinity and Wettability on Oil Recovery Efficiency". *Transp Porous Med* (2009) 76:77-94.

Ayirala, S., Ernesto, U., Matzakos, A., Chin, R., Doe, P., van Den Hoek, P. 2010. "A Designer Water Process for Offshore Low Salinity and Polymer Flooding Applications. SPE 129926.

Alotaibi, M.B. and Nasr-El-Din, H.A. 2010. "Effect of Brine Salinity on Reservoir Fluid Interfacial Tension". SPE paper 121569

Austad, T., Rezaei Doust, A., Puntervold, T. 2010 "Chemical Mechanism of Low Salinity Water Flooding in Sandstone Reservoirs" SPE 129767.

Boussour, S., Cissokho, M., Cordier, P., Bertin, H., Hamon, G. 2009. "Oil Recovery by Low Salinity Brine Injection: Laboratory Results on Outcrop and Reservoir Cores." SPE paper 124277.

Cissokho, M., Boussour, S., Cordier, P., Bertin, H. and Hamon, G., 2009. "Low salinity oil recovery on clayey sandstone: experimental study" presented at the International Symposium of the Society of Core Analysts, Noordwijk aan Zee, Netherland, September.

Jerauld, G.R., Lin, C.Y., Webb, K.J., and Seccombe, J.C., September 2006, Modeling Low-Salinity Waterflooding, SPE 102239, Paper presented at the 2006 SPE Annual Technical Conference and Exhibition, San Antonio, Texas, U.S.A. 24-27.

Lager, A., Webb, K.J., Black, C.J.J., Singleton, M. and Sorbie, K.S., September 2006, Low Salinity Oil Recovery- An Experimental Investigation, SCA paper 2006-36, presented at the International Symposium of the Socitey of Core Analysts, Trondheim, Norway.

Lager, A., Webb, K.J. Collins, I.R. and Richmond, D.M., 2008, LoSal^{TM} Enhanced Oil Recovery: Evidence of Enhanced Oil Recovery at the Reservoir Scale, paper SPE 113976.

Lake, L.W. 1989 *Enhanced Oil Recovery*. 175-181. London: Prentice Hall.

Lee, S.Y., Webb, K.J., Collins, I.R., Lager, A., Clarke, S.M., O'Sullivan, M., Routh, A.F., Wang, X. 2010. "Low Salinity Oil Recovery-Increasing Understanding of the Underlying Mechanisms". SPE 129122.

Ligthelm, D.J., Gronsveld, J., Hofman, J.P., Brussee, N.J., Marcelis, F., and van der Linde, H.A. Novel Waterflooding Strategy by Manipulation of Injection Brine Composition, paper SPE 119835.

McGuire, P. L., Chatman, J.R., Paskvan, F.K., Sommer, D.M. and Carini, F.H.: Low Salinity Oil Recovery: "An Exciting New EOR Opportunity for Alaska's North Slope" SPE paper 93903 presented at 2005 SPE Regional Meeting, Irvine.

Morrow, N.R. et al: "Prospects of Improved Oil Recovery Related to Wettability and Brine Composition", paper presented at the 1996 International Symposium on Evaluation of Reservoir Wettability and Its Effect on Oil Recovery, Montpellier, France, 11-13 September

Pu, H., Xie, X., Yin, P., and Morrow, N.R. " Application of Coalbed Methane Water to Oil Recovery by Low Salinity Waterflooding". SPE paper 113410.

Robertson, E.P. 2007, Low-Salinity Waterflooding To Improve Oil Recovery- Historical Field Evidence, SPE 109965

Seccombe, J.C., Lager, A., Webb, K., Jerauld, G. and Fueg, E., 2008. "Improving waterflood recovery: LoSal^{TM} EOR field evaluation" SPE-113480.

Seccombe, J. Lager A., Jerauld G, Jhaveri B., Buikema, T., Bassler, S., Denis, J., Webb, K., Cockin, A., Fueg, E. "Demonstration of Low-Salinity EOR at Interwell Scale, Endicott Field, Alaska. 2010. SPE 129692.

Skrettingland, K. Holt, T., Tweheyo, M.T., Skjevrak, I. 2010 "Snorre Low Salinity Water Injection-Core Flooding Experiments and Single Well Field Pilot". SPE 129877.

Sposito, G., 1989, *The Chemistry of Soils*: Oxford University Press, Oxford, 275 pp.

Tang, G. and Morrow, N.R., 1997. "Salinity, Temperature, Oil Composition, and Oil Recovery by Waterflooding". 1997. SPE 36680.

Tang, G. and Morrow, N.R., 1999. "Influence of brine composition and fines Migration on crude oil/rock interaction and oil recovery". *J. Pet. Sci. Eng*. **24**: 99-111.

Tang, G. and Morrow, N.R. 2002, "Injection of Dilute Brine and Crude Oil/Brine/Rock Interaction, Environmental Mechanics" Water, Mass and Energy Transfer in Biosphere, Geophysical Monograph 129, pp. 171-179.

Tripathi, I., Mohanty, K.K. "Flow Instability Associated with Wettability Alteration". SPE 110202.

Vledder, P., Fonseca. J.C., Wells, T., Gonzalez, I., Ligthelm, D. 2010. " Low Salinity Water Flooding: Proof of Wettability Alteration on a Field Wide Scale". SPE 129564.

Webb, K.J., Black, C.J.J. and Al-Ajeel, H., April 2003, Low Salinity Oil Recovery- Log-Inject-Log, paper SPE 81460 presented at SPE 13th Middle East Oil Show & Conference, Bahrain 5-8 April.

Webb, K.J., C.J.J. Black and I.J. Edmonds. " The Role of Reservoir Condition Corefloods" *13th European Symposium on Improved Oil Recovery*, Budapest, Hungary, April 2005.

Yildez, H.O. and Morrow, N.R. 1999. "Effect of brine composition on Wettability and Oil Recovery of a Prudhoe Bay Crude Oil, J. Can. Pet. Tech, January, **38** (1) 26-31.

Zhang, Y., Xie, X., and Morrow, N.R. 2007. " Waterflood Performance by Injection of Brine With Different Salinity for Reservoir Cores" SPE 109849.